Global Biogeochemical Cycles

RESEARCH ARTICLE
10.1029/2018GB005994

Flux of Particulate Elements in the North Atlantic Ocean Constrained by Multiple Radionuclides

Christopher T. Hayes[1], Erin E. Black[2], Robert F. Anderson[3,4], Mark Baskaran[5], Ken O. Buesseler[2], Matthew A. Charette[2], Hai Cheng[6,7], J. Kirk Cochran[8], R. Lawrence Edwards[7], Patrick Fitzgerald[8], Phoebe J. Lam[9], Yanbin Lu[10], Stephanie O. Morris[2], Daniel C. Ohnemus[11], Frank J. Pavia[3,4], Gillian Stewart[12,13], and Yi Tang[12,13]

[1]School of Ocean Science and Engineering, University of Southern Mississippi Stennis Space Center, MS, USA, [2]Woods Hole Oceanographic Institution, Woods Hole, MA, USA, [3]Department of Earth and Environmental Sciences, Columbia University, New York, NY, USA, [4]Lamont-Doherty Earth Observatory, Columbia University, Palisades, NY, USA, [5]Department of Geology, Wayne State University, Detroit, MI, USA, [6]Institute of Global Environmental Change, Xi'an Jiaotong University, Xi'an, China, [7]Department of Earth Sciences, University of Minnesota, Minneapolis, MN, USA, [8]School of Marine and Atmospheric Science, Stony Brook University, Stony Brook, NY, USA, [9]Ocean Sciences Department, University of California, Santa Cruz, CA, USA, [10]Earth Observatory of Singapore, Nanyang Technical University, Singapore, [11]Bigelow Laboratory for Ocean Sciences, East Boothbay, ME, USA, [12]School of Earth and Environmental Sciences, Queens College, City University of New York, Flushing, NY, USA, [13]Earth and Environmental Sciences Program, The Graduate Center, City University of New York, New York, NY, USA

Abstract Sinking particles strongly regulate the distribution of reactive chemical substances in the ocean, including particulate organic carbon and other elements (e.g., P, Cd, Mn, Cu, Co, Fe, Al, and ^{232}Th). Yet, the sinking fluxes of trace elements have not been well described in the global ocean. The U.S. GEOTRACES campaign in the North Atlantic (GA03) offers the first data set in which the sinking flux of carbon and trace elements can be derived using four different radionuclide pairs (^{238}U:^{234}Th ;^{210}Pb:^{210}Po; ^{228}Ra:^{228}Th; and ^{234}U:^{230}Th) at stations co-located with sediment trap fluxes for comparison. Particulate organic carbon, particulate P, and particulate Cd fluxes all decrease sharply with depth below the euphotic zone. Particulate Mn, Cu, and Co flux profiles display mixed behavior, some cases reflecting biotic remineralization, and other cases showing increased flux with depth. The latter may be related to either lateral input of lithogenic material or increased scavenging onto particles. Lastly, particulate Fe fluxes resemble fluxes of Al and ^{232}Th, which all have increasing flux with depth, indicating a dominance of lithogenic flux at depth by resuspended sediment transported laterally to the study site. In comparing flux estimates derived using different isotope pairs, differences result from different timescales of integration and particle size fractionation effects. The range in flux estimates produced by different methods provides a robust constraint on the true removal fluxes, taking into consideration the independent uncertainties associated with each method. These estimates will be valuable targets for biogeochemical modeling and may also offer insight into particle sinking processes.

Plain Language Summary Elements, like iron and carbon, are transported from the ocean's surface to its depths on sinking particles. Access to carbon, iron, and other elements is important for marine organisms, which need them to survive. Furthermore, when the organic carbon produced by organisms is transported to depth by sinking, carbon dioxide has been effectively removed from the atmosphere and moved to the deep ocean. This carbon sink is one way that the ocean reduces the heat-trapping potential of the atmosphere. To track how much of a given element descends on particles through the ocean, we use radioisotopes. These are elements that decay at a predictable rate. We can use them like a clock to determine how fast an element is moving from one location to another. Radioisotopes with varying decay rates can tell us about short-term processes, like seasonal blooms, and longer term events, like the impact of ice ages. There were few ocean-scale radioisotope data sets before GEOTRACES expeditions began about 10 years ago. For the first time ever, we present four types of radioisotope data from the U.S. GEOTRACES expedition across the North Atlantic and discuss how it improves our understanding of elemental budgets in the global ocean.

Key Points:
- North Atlantic flux of particulate carbon and trace elements constrained with four radionuclide methods over the entire water column
- Fluxes derived from radionuclide methods at BATS are in agreement with sediment trap fluxes
- C, P, and Cd have biogenic flux profiles; Mn, Co, and Cu have mixed behavior flux profiles; and Fe, Al, and Th-232 have lithogenic flux profiles

Supporting Information:
- Supporting Information S1
- Data Set S1
- Data Set S2
- Data Set S3

Correspondence to:
C. T. Hayes,
christopher.t.hayes@usm.edu

Citation:
Hayes, C. T., Black, E. E., Anderson, R. F., Baskaran, M., Buesseler, K. O., Charette, M. A., et al. (2018). Flux of particulate elements in the North Atlantic Ocean constrained by multiple radionuclides. *Global Biogeochemical Cycles*, *32*, 1738–1758. https://doi.org/10.1029/2018GB005994

Received 4 JUN 2018
Accepted 12 NOV 2018
Accepted article online 22 NOV 2018
Published online 3 DEC 2018

©2018. American Geophysical Union. All Rights Reserved.

1. Introduction

It was discovered in the 1960s that radioactive disequilibria between parent and daughter isotopes in the U and Th decay series could be used to quantify their removal fluxes by particulate matter in the ocean

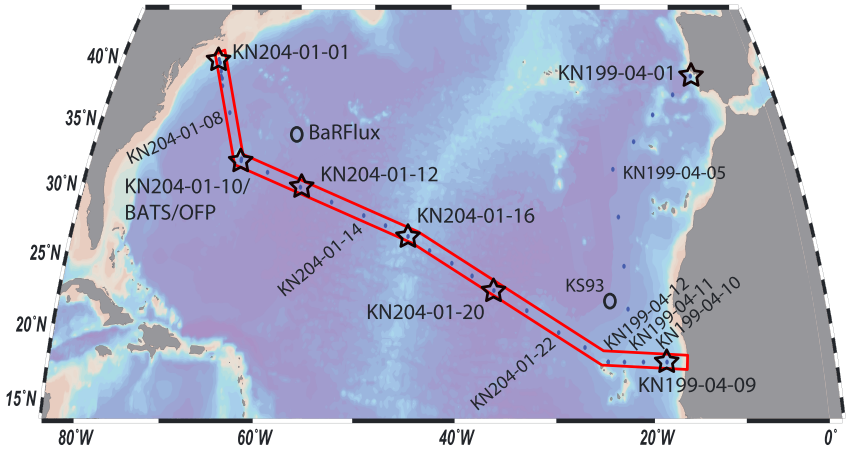

Figure 1. Station location map for sites discussed in this study. The small blue dots indicate all the stations occupied during the GA03 transect, consisting of two cruises KN199-04 and KN204-01, which sailed in 2010 and 2011, respectively. The starred stations indicate the stations for which all four radionuclide pairs that are used in flux determination were measured. Station KN204-01-10 was the GA03 occupation of the Bermuda Atlantic Time-series (BATS) time series site (31°40′N, 64°10′W), which is proximal to the OFP sediment trap site (31°50′N, 64°10′W). Other GA03 stations mentioned in the text are labeled. Station KS93 is another location of a deep sediment trap study of trace element fluxes (Kremling & Streu, 1993). Data from the BaRFlux site reported here were from occupations in 2012 and 2013. The red polygon represents the sections plotted in Figure 2.

(Bhat et al., 1969; Moore, 1969a; Moore & Sackett, 1964; Shannon et al., 1970). This technique is possible when the parent nuclide produces a daughter nuclide that is more rapidly removed by sinking particles than the parent. These pairs, with the half-life given in parentheses after each isotope, include ^{238}U (4.47×10^9 years):^{234}Th (24.1 days), ^{210}Pb (22.3 years):^{210}Po (138 days), ^{228}Ra (5.75 years):^{228}Th (1.91 years), and ^{234}U (2.46×10^5 years):^{230}Th (7.56×10^3 years). For each of the pairs, a removal flux of the more particle-reactive isotope can be quantified using water column profile measurements. When lateral or benthic processes can be neglected, the removal of the particle-reactive nuclide is due to adsorption onto particles sinking through the water column. This sinking flux strongly regulates the distribution of many elements in the ocean, including climate-relevant elements, such as carbon and iron, as well as many other bioactive or geochemical tracer elements.

Sinking fluxes in the ocean were first measured using sediment traps. However, as found in the 1990s, there are difficulties in accurately representing vertical fluxes with sediment traps due to logistical problems, such as trap geometry, local fluid dynamics (e.g., Gardner et al., 1997), and swimmers. The latter are organisms that enter the trap through their own mobility and bias the assessment of passively sinking material (Buesseler et al., 2007a). While sediment trap technology has improved in recent years through the use of neutrally buoyant traps (Buesseler et al., 2007a) and swimmer-exclusion traps (e.g., Hansell & Newton, 1994; Peterson et al., 1993), the indirect radioactive disequilibria techniques to quantify sinking flux are appealing alternatives given that water column measurements can be taken at higher spatial resolution than sediment traps and require only one occupation of a particular location.

In this study of the GA03 U.S. GEOTRACES North Atlantic Transect (Figure 1), we first describe how activity profiles of the four radionuclide pairs can be used to derive removal fluxes of ^{234}Th, ^{210}Po, ^{228}Th, and ^{230}Th, respectively, over different integrated timescales and depth zones of the water column. Then, we will describe the particulate element/radionuclide ratios that are applied to radionuclide fluxes to derive sinking elemental fluxes. Finally, we will derive the suite of sinking elemental fluxes (C, P, Cd, Mn, Cu, Co, Fe, Al, and ^{232}Th) using all four radionuclide methods. This group of elements was selected for two reasons. First, these elements range in the degree to which they participate in biological, lithogenic, or authigenic particle cycling (Ohnemus, 2014; Ohnemus & Lam, 2015), and second, for these elements there are existing sediment trap data from the North Atlantic (Huang & Conte, 2009; Kremling & Streu, 1993) against which to compare our radionuclide-derived fluxes. Using the methodology presented in this paper and published data, additional particulate fluxes can be derived for the GA03 for Ag, Ba, Nd, Ni, Pb, Ti, V, and Y, but these are beyond the scope of this paper.

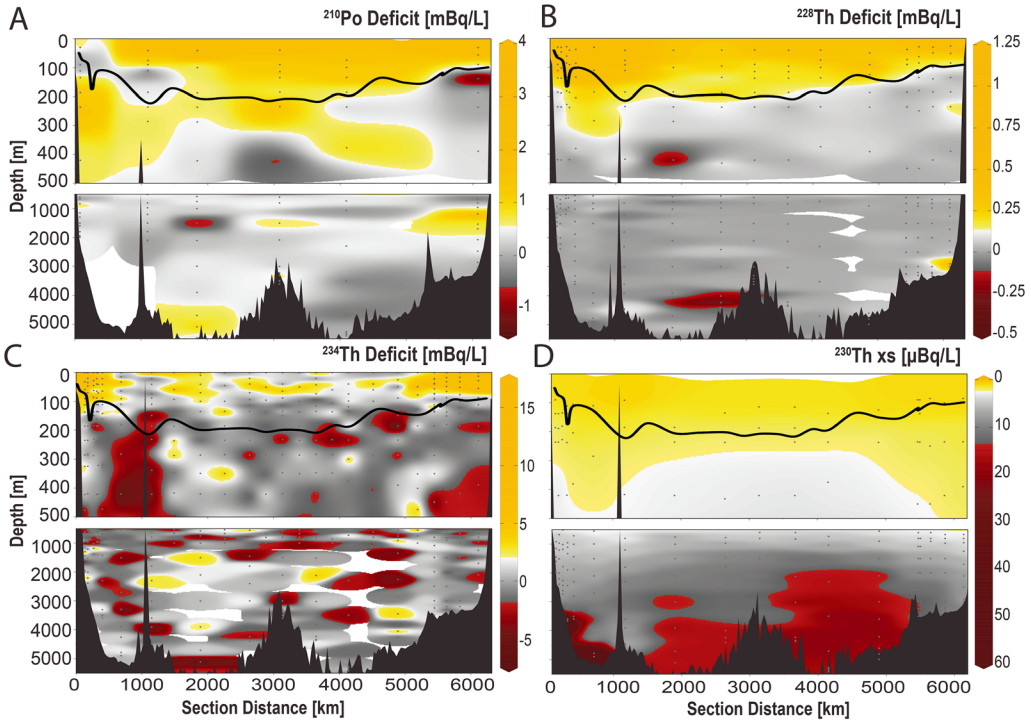

Figure 2. Section plots of radionuclide deficits across the GA03 transect defined in Figure 1. (a) Values are defined as total ^{210}Pb minus total ^{210}Po activity (so that a ^{210}Po deficit is positive). (b) Values are defined as total ^{228}Ra minus total ^{228}Th activity. (c) Values are defined as total ^{238}U (based on salinity) minus total ^{234}Th. (d) The total ^{230}Th xs activity in seawater, which is the measured ^{230}Th corrected for ^{230}Th added to the water column by lithogenic material. In a–c, the color bars are designed to emphasize daughter radionuclide deficits (in yellow), near secular equilibrium (in gray), or daughter radionuclide excesses (in red). For ^{230}Th, its deficit with respect to ^{234}U is nearly complete (would be about 50 mBq/L), and therefore, only the ^{230}Th activity is plotted. Note differing depth scales for the upper 500 m and for 500- to 5,000-m depth. The black lines across the upper section denote the depth of the primary production zone, as defined by fluorescence profiles (Owens et al., 2015). For comparison to Figure 1, KN204-01-10 and KN199-04-09 correspond with 1,000- and 6,000-km section distance, respectively.

2. Background

2.1. The ^{234}Th Flux Method

The ^{234}Th-^{238}U disequilibrium method has been developed over many decades for estimating particle export in the upper ocean over time scales of weeks to months (e.g., Benitez-Nelson et al., 2001; Buesseler et al., 1992, 2009; Coale & Bruland, 1987). In seawater, daughter product ^{234}Th is highly particle reactive, while parent ^{238}U is conservative with respect to salinity (Ku et al., 1977; Owens et al., 2011). Water column ^{234}Th deficits (seawater ^{234}Th/^{238}U activity ratios <1) are indicative of a rate of ^{234}Th scavenging and sinking removal that significantly exceeds the rate of ^{234}Th radioactive decay (half-life 24.1 days). Thorium-234 deficits from the GA03 transect have been described (Lerner et al., 2016, 2017; Owens et al., 2015), and they typically appear in the upper few hundred meters of the water column (Figure 2c), where particle flux is large enough to induce a radioactive disequilibrium. Below the upper few hundred meters of the water column and outside of benthic nepheloid layers or hydrothermal plumes, deep water ^{234}Th is typically at secular equilibrium with ^{238}U.

Where ^{234}Th deficits exist, they can be integrated to estimate a ^{234}Th removal flux, F(^{234}Th), as a function of integration depth, from the surface to depth, z (equation (1)). In this equation, total (dissolved plus particulate) ^{234}Th activity is used and ^{238}U activity is estimated based on salinity and the salinity-uranium relationship defined by Owens et al. (2011).

$$F\left(^{234}Th\right)_z = \int_0^z \lambda_{234}\left(^{238}U - ^{234}Th\right)\, dz \quad (1)$$

Here λ_{234} is the decay constant of ^{234}Th (10.51/year). The appropriate depth of integration is important to carefully consider. Prior studies have used either a fixed depth over which to compute the deficit (e.g., 150 m), or a variable depth informed by particle processes, such as the euphotic zone or the primary production zone, which is defined by the depth at which fluorescence has attenuated to 10% of its surface value (Owens et al., 2015; Puigcorbé et al., 2017). Here rather than choose a standard depth, we will report fluxes at the depths for which we have particulate measurements. For ^{234}Th specifically, we chose to integrate from the surface to the base of the primary production zone as described by Owens et al. (2015). Of course, equation (1) assumes no physical circulation effects on ^{234}Th inventories or temporal changes in ^{234}Th activities due to changing fluxes (steady state assumption; Savoye et al., 2006). *Nonsteady state* models for ^{234}Th flux have been developed (e.g., Buesseler et al., 1995) in which known temporal variability in ^{234}Th activity is used to estimate the impact on ^{234}Th fluxes. In general, the steady state assumption results in an underestimate of the true ^{234}Th flux during conditions of decreasing ^{234}Th activities, and vice versa for conditions of increasing ^{234}Th activities. Under certain circumstances, physical transport may also affect ^{234}Th budgets and the fluxes derived from them. For instance, upwelling of water with a high ^{234}Th activity would reduce the apparent ^{234}Th deficit and thus underestimate the true ^{234}Th flux, when upwelling is ignored. In this study, we cannot assess the nonsteady state model because of a lack of time series observations. Neither do we include the impact of upwelling, which has been shown to be significant at some locations and times, for example, in situations of equatorial or coastal upwelling (Bacon et al., 1996; Black et al., 2018; Buesseler et al., 1998; Murray et al., 1996), neither of which apply at the GA03 stations described here.

The GA03 data can be compared with ^{234}Th flux data collected near the Bermuda Rise (BaRFlux site, 33°40′N, 58°W) during May and August 2012 and June 2013. These data have not been reported previously, and full methods and documentation for this project are provided in the supporting information. BaRFlux is about 620 km to the northeast of the Bermuda Atlantic Time-series (BATS) station, which was occupied during GA03 as station KN204-01-10 (see Figure 1). The BaRFlux and BATS sites are likely comparable in terms of particle flux, as both sites are in the oligotrophic subtropical gyre.

2.2. The ^{210}Po Flux Method

Polonium-210 is produced by decay of ^{210}Pb, via a short-lived intermediate (^{210}Bi, half-life 5 days). This radionuclide pair has been used to estimate particle export in the upper water column, analogously to the ^{234}Th method (e.g., Bacon et al., 1976; Murray et al., 2005; Nozaki et al., 1976; Stewart et al., 2007). In contrast to ^{238}U, the parent ^{210}Pb is nonconservative and nonuniform in the ocean. Lead-210 is produced in situ in seawater from decay of its soluble grandparent ^{226}Ra (half-life 1600 years) through a series of short-lived intermediates. In addition, ^{238}U-series decay occurring in the continental crust releases gaseous ^{222}Rn (half-life 3.8 days) to the atmosphere, which subsequently decays to ^{210}Pb (through a series of short-lived Po and Pb isotopes, half-lives $<$ 30 min). An excess of ^{210}Pb relative to ^{226}Ra (^{210}Pb/^{226}Ra $>$ 1) is present in seawater in the upper water column due to the additional atmospheric input of activity via wet and dry deposition of aerosols laden with ^{210}Pb (Baskaran, 2011; Moore et al., 1974; Turekian et al., 1977). Pb is a particle-reactive element, and its residence time with respect to scavenging in the surface ocean is about 2 years (Bacon et al., 1976; Nozaki et al., 1976). It is sometimes possible to calculate a removal flux of ^{210}Pb based on a ^{210}Pb deficit with respect to its soluble parent ^{226}Ra. However, in GA03, ^{210}Pb activities were found to be in excess of ^{226}Ra throughout the entire section in the upper 1,000 m (Rigaud et al., 2015), making an estimate of the sinking ^{210}Pb flux impossible to extract.

There is, however, an upper water column deficit of ^{210}Po activity with respect to ^{210}Pb activity (Figure 2a), presumably due to preferential sorption and particle export of ^{210}Po. Additionally, laboratory culture studies demonstrate that Po is not only scavenged or adsorbed onto particle surfaces (like Pb and Th) but that an active uptake of Po into cells also occurs (Fisher et al., 1983; Stewart et al., 2005). Thus, ^{210}Po flux may be carried within sinking cells to a greater degree than ^{234}Th (Verdeny et al., 2009). In fact, both Pb and Po may have specific affinities for different particle types. Using GA03 data, it was determined that ^{210}Po has stronger associations with particulate $CaCO_3$ and particulate organic matter, while ^{210}Pb had stronger associations with opal and lithogenic phases (Tang et al., 2017). Additionally, the longer half-life of ^{210}Po (138 days) versus ^{234}Th (24.1 days) means that ^{210}Po flux reflects a longer integration time of particle flux events than does ^{234}Th flux. The removal flux of ^{210}Po is defined by equation (2).

$$F\left(^{210}Po\right)_z = \int_0^z \lambda_{Po}\left(^{210}Pb - ^{210}Po\right)\, dz \quad (2)$$

Here λ_{Po} is the decay constant of ^{210}Po (1.829/year), and the activities of both radionuclides are total (dissolved + particulate) activities. The ^{210}Pb/^{210}Po distribution in GA03 has been described (Rigaud et al., 2015; Tang et al., 2017). A nonsteady state model can also be employed to assess the influence of temporal changes in ^{210}Pb and ^{210}Po activities on derived ^{210}Po fluxes, but we cannot attempt this here since no time series observations were made. The bias in derived flux would be qualitatively similar to that described above for the time-varying ^{234}Th/^{238}U disequilibria: the true flux would be underestimated during times of decreasing ^{210}Po activity and vice versa.

The depth of integration is also an important consideration for ^{210}Po fluxes. As with ^{234}Th, the largest ^{210}Po deficits exist in the euphotic zone. Surprisingly, however, in the North Atlantic, ^{210}Po deficits persist into the deep water (Hong et al., 2013; Kim & Church, 2001; Rigaud et al., 2015; Figure 2) and scavenging of ^{210}Po compared to ^{210}Pb may happen throughout the water column. It is not clear that deep ^{210}Po deficits necessarily represent the sinking removal of ^{210}Po or some effect of differential Pb/Po scavenging, biological uptake, remineralization, and/or possible analytical biases (Church et al., 2012; Kim, 2001). Therefore, in this study we will only examine ^{210}Po fluxes from the surface to the base of the primary production zone.

2.3. The ^{228}Th Flux Method

Another thorium isotope, ^{228}Th, is produced by decay of ^{228}Ra, which in turn is a decay product of primordial ^{232}Th. On the time scale of upper ocean export production, ^{228}Ra is unreactive in seawater. However, unlike ^{238}U, it is not uniformly distributed in the water column; rather, ^{228}Ra is elevated in the surface ocean and near the seafloor due to dispersion from shelf and deep-sea sediment pore waters, enriched from ^{232}Th decay (Moore, 1969b). Further, ^{228}Ra is not supported by ^{232}Th in the water column. Disequilibria between ^{228}Th and ^{228}Ra have been interpreted in terms of scavenging removal in the GEOSECS (Li et al., 1980) and JGOFS (Luo et al., 1995) ocean chemistry campaigns. Only a few studies have derived ^{228}Th deficit-based particulate fluxes (Lepore & Moran, 2007; Okubo et al., 2007). This is because the low open ocean abundance of sediment-sourced ^{228}Ra (half-life 5.8 years) makes it challenging to measure this nuclide and its daughter ^{228}Th with sufficient accuracy. Additionally, because of the half-life of ^{228}Th, 1.9 years, it has been argued that circulation effects may significantly overprint particle flux processes (Luo et al., 1995). As a result, there have been relatively few studies that compare ^{228}Th-derived particulate fluxes to other flux methods, as we can here. Data from GA03 have been discussed for ^{228}Ra (Charette et al., 2015) and ^{228}Th (Lerner et al., 2016, 2017; Maiti et al., 2015). A similar integrated formula describes ^{228}Th flux (equation (3)), where λ_{228} = 0.363/year, and total activities are used for the radionuclides.

$$F\left(^{228}Th\right)_z = \int_0^z \lambda_{228}\left(^{228}Ra - ^{228}Th\right)\, dz \quad (3)$$

The proper depth of integration is also an important question for the ^{228}Th/^{228}Ra pair. The longer half-life of ^{228}Th, in comparison to ^{234}Th and ^{210}Po, results in a longer timescale of integration of particle flux. Furthermore, ^{228}Th is expected to be more sensitive to the smaller particle fluxes below the primary production zone. In this study, we will integrate from surface to the depth at which secular equilibrium is reached, which generally occurs around 600 m or shallower in GA03 (Figure 3b). Once secular equilibrium is reached, we assume that this radionuclide pair is no longer sensitive to the smaller particle fluxes of the deeper water column. Additionally, ^{228}Ra activities are usually quite low in the midwater column (Charette et al., 2015), far from shelf ^{228}Ra sources, so that it is difficult to quantify disequilibrium without an unacceptably high degree of uncertainty.

2.4. The ^{230}Th Flux Method

Since the half-life of ^{230}Th (76,000 years) is much longer than its residence time in the ocean (decades), there is enough time for scavenging to remove nearly all of the ^{230}Th from the water column (Moore & Sackett, 1964). Activity ratios of total ^{230}Th to its parent ^{234}U in GA03 seawater are all less than ~0.00002. Consequently, one can assume that at any point in the water column, particles are carrying downward all of the overlying production of ^{230}Th by ^{234}U decay (equation (4)). This assumption is commonly made for reconstructing sedimentary fluxes (François et al., 2004) and has recently been employed for water column

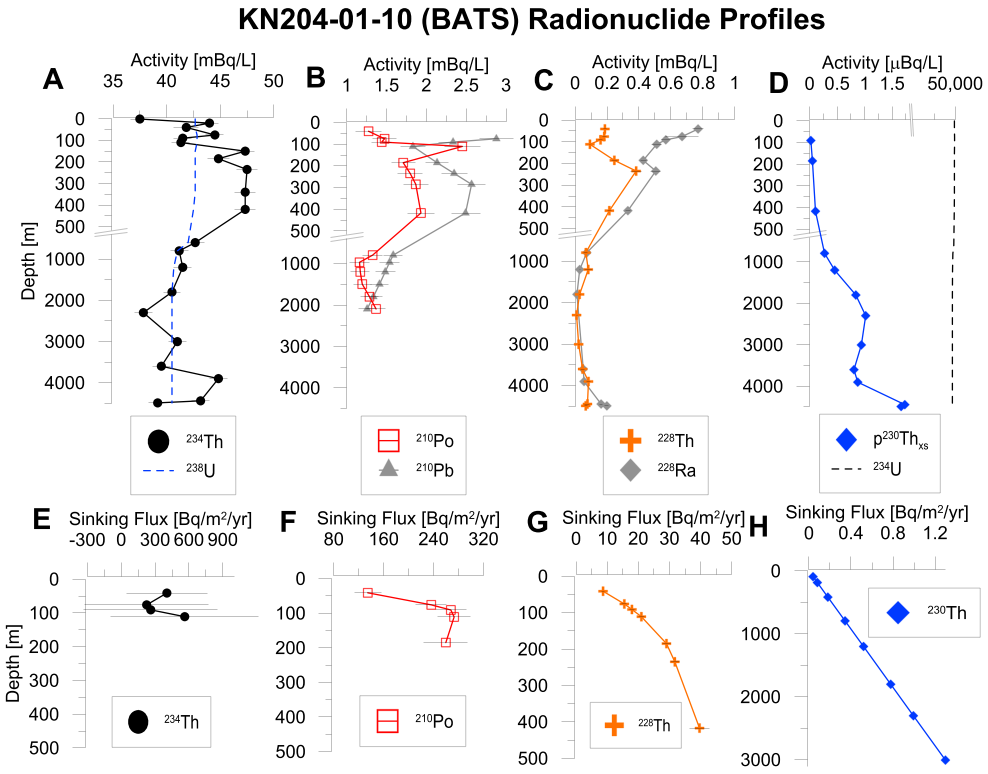

Figure 3. Radionuclide activity profiles of (a) total ^{234}Th (black circles) compared with dissolved ^{238}U based on salinity, (b) total ^{210}Po (red squares) and total ^{210}Pb (gray triangles), (c) total ^{228}Th (orange crosses) and total ^{228}Ra (gray diamonds), and (d) particulate ^{230}Th xs (blue diamonds) compared with dissolved ^{234}U based on salinity and the global uranium isotopic composition of seawater. (e) Sinking flux of ^{234}Th based on the integrated deficit between total ^{234}Th and ^{238}U activities. (f) Sinking flux of ^{228}Th based on the integrated deficit between total ^{228}Th and ^{228}Ra activities. (g) Sinking flux of ^{210}Po based on the integrated deficit between total ^{210}Po and ^{210}Pb activities. (h) Sinking flux of ^{230}Th based on the integrated production due to ^{234}U decay. Note different depth scales in subplots. The error bars represent 1 sigma uncertainty, and, if they are not visible, they are smaller than the symbol size.

fluxes (Anderson et al., 2016; Hirose, 2006). In this study, activities of ^{234}U are estimated from measured salinity, the Owens et al. (2011) salinity-U relationship, and the globally uniform ^{234}U/^{238}U activity ratio of seawater, 1.1468 (Andersen et al., 2010).

$$F\left(^{230}Th\right)_z = \int_0^z \lambda_{230}{}^{234}U\, dz \tag{4}$$

Circulation may impact ^{230}Th distributions in seawater, including vertical redistribution due to upwelling (Luo et al., 1995) or lateral redistribution to areas of high scavenging removal, termed boundary scavenging (Roy-Barman, 2009). In the GA03 transect, about 40% of the water column production is redistributed laterally from the area around the Cape Verde islands toward the high-particle-flux Mauritanian margin (Hayes et al., 2015a). Lateral redistribution is likely much less than 40% in the rest of the GA03 transect, which has much smaller lateral gradients in particle flux (Owens et al., 2015). Since ^{230}Th activities increase with depth in the water column (Hayes et al., 2015a), most of its inventory is in the deep ocean (>1,500-m depth). Thus ^{230}Th-based fluxes are much less sensitive to upwelling than for the shorter-lived radionuclides. Water column ^{230}Th fluxes reflect average fluxes over the timescale it takes particles to sink throughout the water column, years to decades (Bacon & Anderson, 1982). Water column ^{230}Th fluxes can be integrated over the entire water column. Here we integrate to the depths at which we have particulate ^{230}Th data. However, benthic processes, such as sediment resuspension or scavenging from hydrothermal vents appear to impact ^{230}Th distributions up to about 1 km above the seafloor (Hayes et al., 2015a; Pavia et al., 2018). Therefore, we do not interpret ^{230}Th-based fluxes below about 3-km depth at BATS and in benthic waters at other stations where nepheloid layers (or hydrothermal plumes) are present.

Because of its very low activity in seawater, the particulate ^{230}Th supported by decay of particulate ^{234}U found within minerals (lattice-bound) in the water column can be significant compared to the particulate ^{230}Th scavenged from the water column. It is only the flux of ^{230}Th sourced from dissolved ^{234}U decay that we can predict using equation (4). This fraction of the particulate ^{230}Th is termed *particulate ^{230}Th xs*. In GA03 the percentage of particulate ^{230}Th supported by mineral-bound ^{234}U ranged from 0 to 60%, averaging 11% (Hayes et al., 2015b). Throughout this manuscript, whenever particulate ^{230}Th is mentioned, we are referring to the corrected data, particulate ^{230}Th xs, but the *xs* is omitted for simplicity. The supported fraction of the shorter-lived isotopes is negligible and is ignored.

The integrations described with equations (1)–(4) were done using trapezoidal integration between measured values. Between the shallowest sample (generally 30- to 100-m depth) and the surface (0-m depth), it was assumed that the surface had the same radionuclide activity as the shallowest sample.

2.5. Converting Radionuclide Fluxes Into Elemental Fluxes

For each method discussed above, the radionuclide flux ($F(X)$) can be converted into the flux of another element, $F(Z)$, by multiplying by the ratio of the concentration of element (Z) to the activity of nuclide (X) of the particulate material responsible for transporting the elements downward in the water column, $(Z/X)_p$ (equation (5)).

$$F(Z) = F(X) \times \left(\frac{Z}{X}\right)_p \tag{5}$$

There are practical limitations for collecting material to characterize $(Z/X)_p$ (Buesseler et al., 2006; Smith et al., 2014; Weinstein & Moran, 2005). Ideally, a sediment trap would collect the exact class of particles responsible for sinking removal, assuming unbiased collection, and deployment time sufficient to characterize temporal variability. Particles can also be collected during a single station occupation by filtration of water samples collected with water collection devices, such as GO-FLO bottles. However, water collection devices are generally limited to a volume of ~30 L, which is insufficient to analyze most of the radionuclides employed here. In situ pumps, on the other hand, can collect particle samples during a single station occupation from a much larger volume of water within a reasonable time period (hundreds of liters per hour). One disadvantage of both GO FLO-filtered and in situ pump-filtered particles is that the size spectrum of these particles likely reflects a mixture of sinking and nonsinking particles, whereas sediment traps generally collect only sinking particles.

On GA03, sediment traps were not deployed. Both in situ pumped (Lam et al., 2015; Ohnemus & Lam, 2015) and GO FLO-bottle-filtered (Twining, Rauschenberg, Morton, Ohnemus, et al., 2015) particles were collected. GO-FLO particles were analyzed only for a subset of the cruise track. Therefore, we use the more extensive data from the in situ pumped particles to define (Z/X) ratios. Size-fractionated particulate samples were collected using a 51-μm prefilter placed on top of either paired quartz fiber filters (Whatman QMA) or paired 0.8-μm Supor filters (Lam et al., 2015). Particles collected on the 51-μm filter therefore represent the >51-μm size class, or the large size fraction (LSF). Generally using only the top of the paired filtered for analysis, it has been determined that both QMA and Supor paired filters collect the 1- to 51-μm size class, or the small size fraction (SSF), with the Supor filter likely containing particles as small as 0.8 μm (Bishop et al., 2012; Lam et al., 2015; Ohnemus & Lam, 2015). The BaRFlux project used a slightly larger pore size pre-filter (70 μm) to separate the LSF and SSF (see the supporting information).

We do not know the true size spectrum of sinking particles for each of the timescales relevant to the radionuclides pairs studied here. However, if both large and small particles can be analyzed, it can be determined how sensitive the flux estimate is to this uncertainty. With data available from GA03, we can directly compare the ratios in the LSF and SSF for ^{234}Th (Owens et al., 2015) and ^{210}Po (Rigaud et al., 2015), using the particulate trace element (Ohnemus & Lam, 2015) and particulate organic carbon (POC) (Lam et al., 2015) data from those same size fractions. For ^{230}Th, small particle samples were analyzed for the entire section and only a subset of large particle samples was analyzed. For ^{228}Th, small particle samples were analyzed for the entire section, and a subset of large particle samples was analyzed, but two to three large particle samples had to be combined to make a large enough sample for adequate analytical statistics.

3. Results

3.1. Radionuclide Activities and Fluxes

Because of all the historical data available from this site, we focus our comparison on station KN204-01-10, co-located with BATS, occupied in November 2011. During this occupation, there was little ^{234}Th deficit in the primary production zone (Figures 3a and 2c), which at this station was 197-m deep, and a relatively large excess of ^{234}Th activity at 200- to 500-m depth. This large ^{234}Th excess is often a sign of ^{234}Th regeneration from particles (Maiti et al., 2010); however, a regeneration signal is not likely in this case since a correspondingly large ^{234}Th deficit is not seen in surface waters, which would be required by a one-dimensional mass balance. Therefore, this ^{234}Th excess is more likely an advective feature. Satellite estimates of net primary productivity (CbPM algorithm, www.science.oregonstate.edu/ocean.productivity/) in the KN204-01-10 region for the four 8-week periods prior to sampling range from 24.0 to 28.8 mmol C/m^2/day (cf. annual climatological range of 20 to 85 mmol C/m^2/day), indicating no significant blooms during this time that could have generated a surface ^{234}Th deficit.

The ^{234}Th flux (equation (1)) integrated to 150 m is 560 ± 650 Bq/m^2/year (Figure 3e) and becomes negative at 200 m (not plotted in Figure 3e) because of the large excess ^{234}Th activity at depth. For comparison, there have been several times series studies of ^{234}Th flux at BATS, which observed 150-m-integrated ^{234}Th fluxes of 610–7,900 Bq/m^2/year (n = 6) during October 1996–August 1997 (Kim & Church, 2001) and from zero (or negative deficit) to over 14,000 Bq/m^2/year (n = 30) during 1993–1995 (Sweeney et al., 2003). This puts the KN204-01-10 ^{234}Th flux observation at the low end but well within the observed range. Interestingly, however, the GA03 stations immediately to the east and west of KN204-01-10 had larger primary production zone ^{234}Th fluxes (2,920 ± 970 and 1,740 ± 590 Bq/m^2/year, respectively; Owens et al., 2015) and smaller ^{234}Th excesses (Figure 2c). Therefore, the negligible KN204-01-10 ^{234}Th deficit may be associated with a mesoscale feature.

The ^{210}Pb activity profile (Figure 3b) indicates input from atmospheric deposition, with highest activities in the upper 500 m, as seen in previous North Atlantic surveys (Bacon et al., 1976). At KN204-01-10, samples were only taken in the upper 2 km of the water column. There is a ^{210}Po deficit throughout most of the upper 1.5 km at KN204-01-10, except for the one sample at 110 m, which indicates a clear ^{210}Po excess, as also described by Rigaud et al. (2015). This is the same depth at which the ^{234}Th excess becomes apparent (Figure 3a). At this depth, particle dissolution via respiration processes is likely leading to the release of scavenged ^{210}Po back into the water column after particle export close to the base of the euphotic zone. Excesses of ^{210}Po activity at or near euphotic zone depths are also apparent in prior North Atlantic studies (Bacon et al., 1976; Hong et al., 2013). The calculated sinking flux of ^{210}Po at KN204-01-10 of 130–270 Bq/m^2/year (Figure 3f) for the upper 150 m is comparable to, and slightly higher than, the range seen in the BATS time series observations during 1996 — 1997 of 50–190 Bq/m^2/year (average 125 Bq/m^2/year; Kim & Church, 2001).

The ^{228}Ra activity profile has its largest values in the upper 500 m of the water column of KN204-01-10 (Figure 3c) likely due to mixing with water in contact with North American margin sources, such as continental shelf sediments and submarine groundwater discharge (Charette et al., 2015; Moore et al., 2008). The ^{228}Th profile shows a deficit with respect to ^{228}Ra activity throughout the upper 500 m. Below this depth, ^{228}Ra activities decrease to very low levels, such that any disequilibrium with respect to ^{228}Th is difficult to measure with any reasonable level of uncertainty. The integrated ^{228}Th fluxes (calculated using equation (3)) increase with depth, with a slight inflection point of more slowly increasing fluxes around 200 m (Figure 3g). Li et al. (1980) reported ^{228}Th fluxes integrated to 350 m of 12–19 Bq/m^2/year at sites nearby KN204-01-10 (GEOSECS stations 29 and 120, at 35°58.5′N, 47°00.5′W and 33°16′N, 56°33′W), which are comparable to, but smaller than, the roughly 30 Bq/m^2/year measured at KN204-01-10.

Finally, the particulate ^{230}Th profile from KN204-01-10 demonstrates increasing activities with depth, consistent with the model of reversible scavenging (Bacon & Anderson, 1982). The sinking ^{230}Th flux (Figure 3h) increases linearly with depth, as this is simply the integrated production by conservative ^{234}U. At a nearby site (32°5′N, 64°15′W), Bacon et al. (1985) measured an annual average ^{230}Th flux of 1.0 Bq/m^2/year in a 3,200-m sediment trap, which is within 40% of the predicted ^{230}Th production rate integrated to this depth of 1.38 Bq/m^2/year. This small apparent deficit of ^{230}Th flux from that trap may have been related to

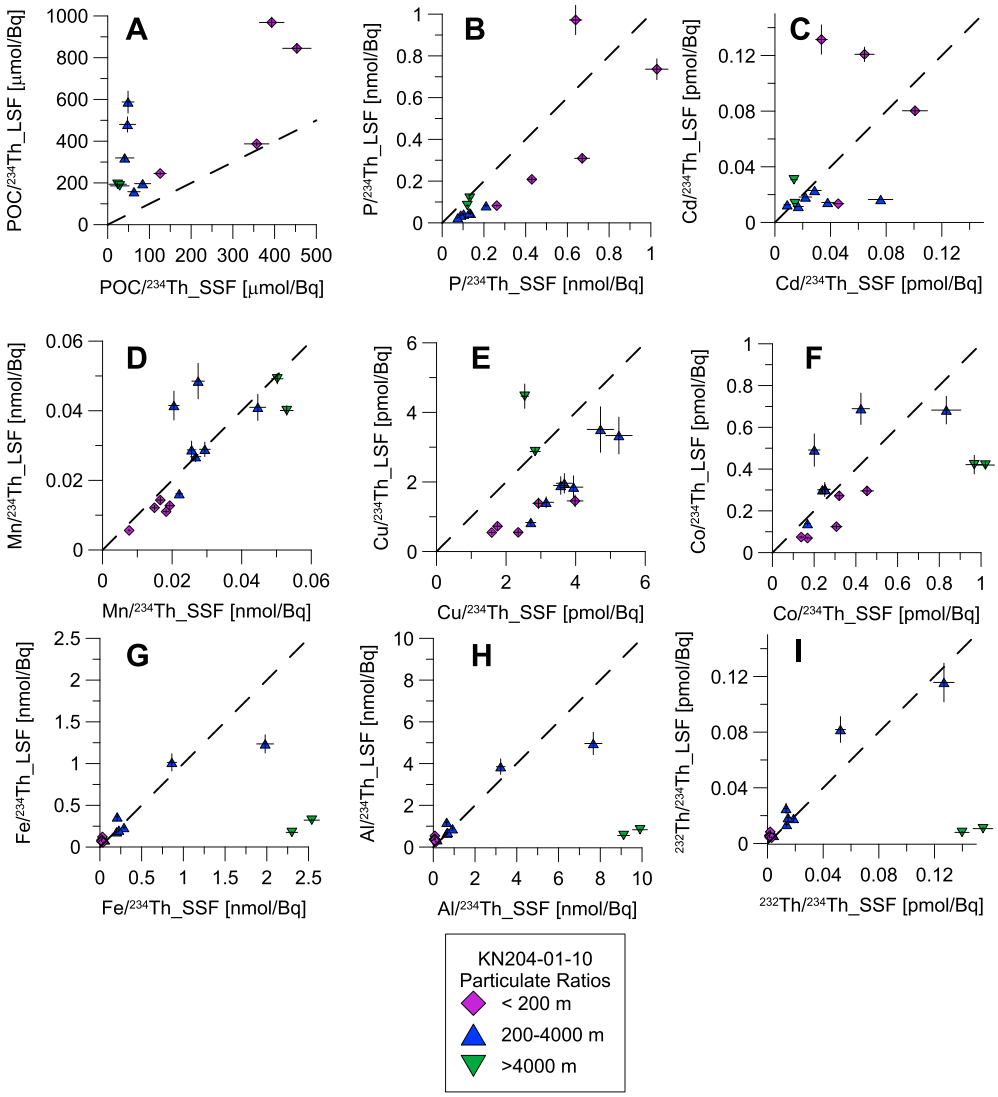

Figure 4. Cross plots of element concentration to ^{234}Th activity ratios in large size fraction (LSF, >51 μm) of particles against the ratios in small size fraction (SSF, 1–51 μm) of particles from station KN204-01-10.

undertrapping of particles or lateral transport of ^{230}Th away from the BATS site. Modeling studies (Henderson et al., 1999) conclude, and observational studies (Hayes et al., 2015a) support, the view that in most of the ocean the sinking flux of ^{230}Th is within about 30% of its overlaying production due to uranium decay. Thus, uncertainties related to water column redistribution of ^{230}Th are likely less than 30%. At roughly 3-km depth and below at this location, the dissolved ^{230}Th begins to decrease with depth (Hayes et al., 2015a), reflecting enhanced removal of ^{230}Th by scavenging onto resuspended particles of an extended nepheloid layer at the BATS location (Lam et al., 2015; Sherrell & Boyle, 1992). Particulate ^{230}Th activities also decrease below 3 km (Figure 3d), until the two near-bottom samples where it appears there are resuspension of particles with scavenged ^{230}Th. Caution should be taken when interpreting ^{230}Th in nepheloid layer locations, as the conditions of reversible scavenging may not hold.

3.2. Particulate Element to Radionuclide Ratios

Ratios of the concentration of elements of interest (C, P, Cd, Mn, Cu, Co, Al, Fe, and ^{232}Th) to ^{234}Th and ^{210}Po activities in the small (1–51 μm) and large (>51 μm) particulate phases for KN204-01-10 are plotted in Figures 4 and 5. The ratios of POC to ^{234}Th and ^{210}Po are significantly higher in the LSF than in the SSF

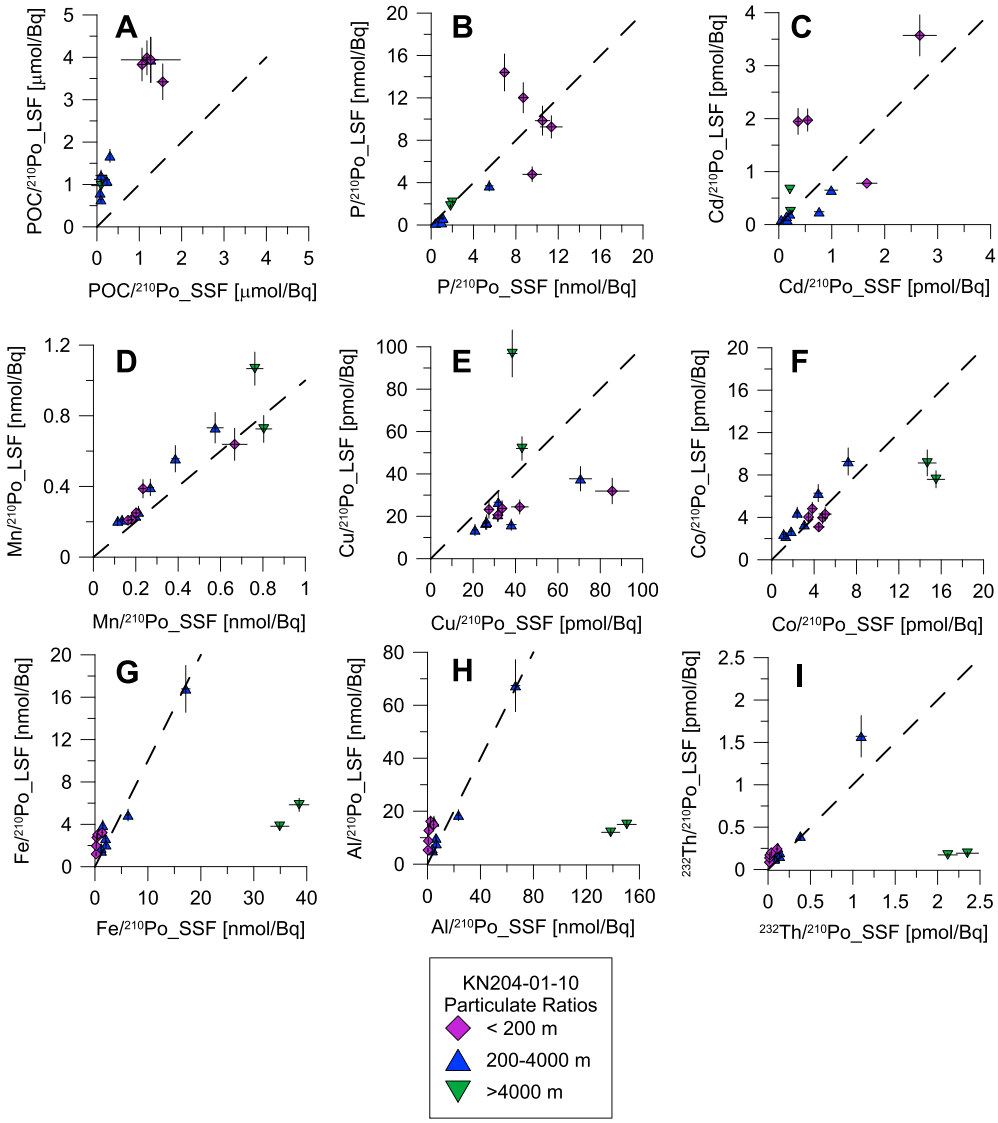

Figure 5. Cross plots of element concentration to ^{210}Po activity ratios in large size fraction (LSF, >51 μm) of particles against the ratio in small size fraction (SSF, 1–51 μm) of particles from station KN204-01-10.

(Figures 4a and 5a), by factors of 2–10 for individual samples. This is generally due to a greater difference in ^{234}Th and ^{210}Po activities between the two size classes than the difference in POC concentrations. The radionuclides have a higher specific activity in the small phase, likely because these small particles have a larger surface area per unit mass, onto which the radionuclides are sorbed. POC concentration to ^{234}Th activity ratios are also generally higher in the LSF than in the SSF in the time series observations from the BaRFlux site (see Figure S2 and Data Set S1).

In contrast to POC, P, and Cu appear to have higher element to radionuclide activity ratios in the small particle phase (Figures 4b, 4e, 5b, and 5e), by factors of 1.5–3. The enrichment of P and Cu in the SSF may reflect the much greater proportional abundance there, relative to the LSF, of small prokaryote cells that are enriched in P and Cu (Ohnemus et al., 2017; Twining, Rauschenberg, Morton, & Vogt, 2015). Furthermore, biologically mediated aggregation of small P-rich particles may lead to a depletion of P relative to radionuclides in the LSF compared to the SSF. On the other hand, P in plankton tows has also been shown to be particularly labile (Collier & Edmond, 1984), and thus, P in large particles may be systematically more labile than in small particles. The relative enrichment of P and Cu in the small particles must more than compensate for the greater activity of ^{234}Th and ^{210}Po in the small phase due to the increased surface area of small particles.

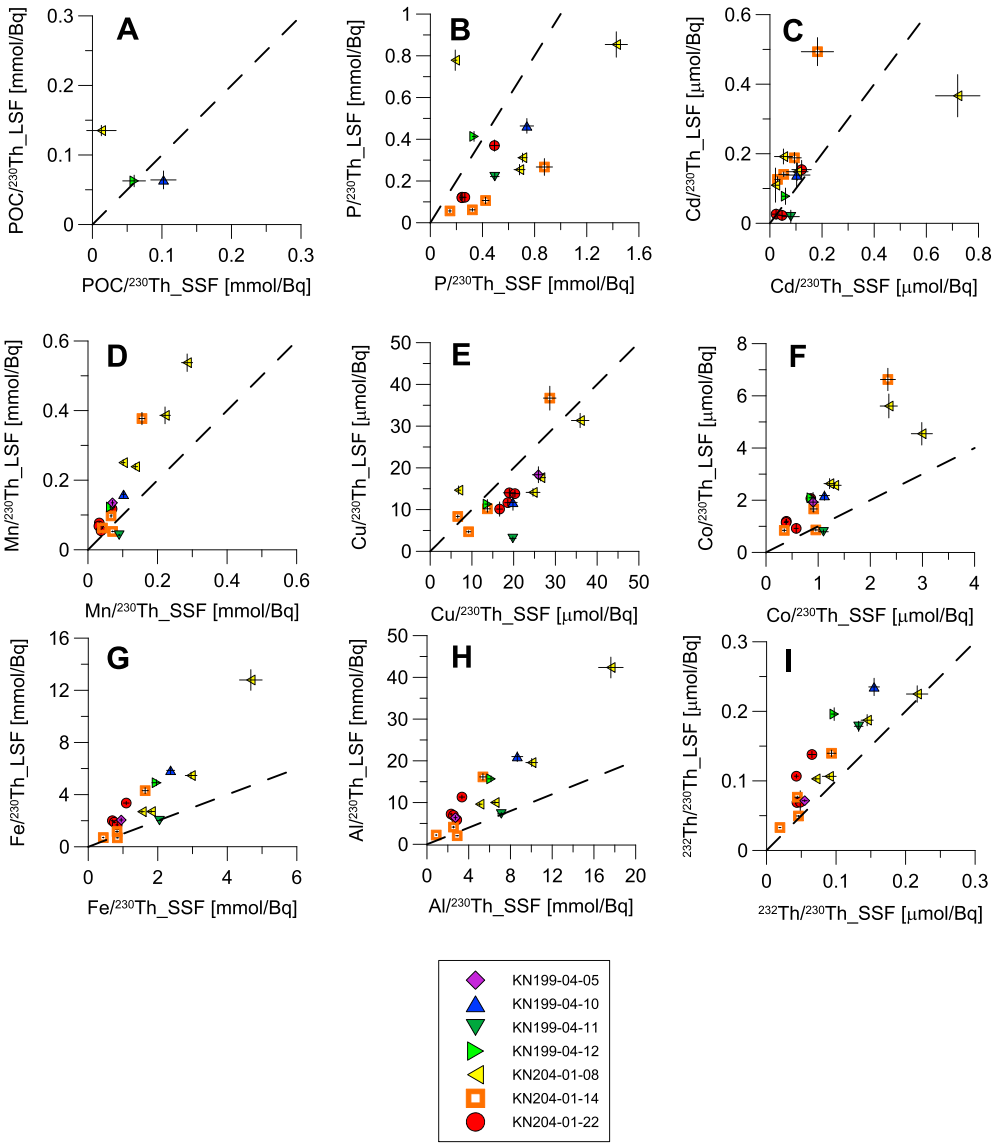

Figure 6. Cross plots of element concentration to ^{230}Th activity ratios in large, sinking particles against the ratios in small particles from select stations from GA03. Samples from KN199-04 were collected from 2-km depth. Samples from KN204-01 were collected from depths ranging between 966 and 4,800 m. The dotted lines indicate the 1-to-1 line.

Cadmium, Mn, and Co have similar ratios of concentration to activity of the short-lived radionuclides in the two size classes, within about 40% (Figures 4 and 5). This result may have implications for what fraction of these elements is adsorbed versus contained within cell or mineral lattice. In terms of estimating fluxes, however, the use of either large or small particle ratios has relatively small impact for these elements.

Finally, ratios of Al and Fe concentration to ^{234}Th and ^{210}Po activity are higher in the LSF than in the SSF within the upper 200 m of the water column (Figures 4g, 4h, 5g, and 5h), the large particles having a higher ratio by factors of 1–13. LSF and SSF elemental to radionuclide ratios are similar for Fe, Al, ^{234}Th, and ^{210}Po in the rest of the water column (1- to 4-km depth), excluding the benthic nepheloid layer.

The LSF/SSF comparison for particulate element concentration to ^{230}Th activity ratios can be made on a select number of deep water (966 to 4,800 m) samples from various GA03 stations (Figure 6). Large particulate ^{230}Th activities for the seawater volumes collected by in situ pump on GA03 were expected to be close to the detection limit, especially for shallow water samples. Thus, in this first U.S. GEOTRACES transect, only a selection of deep water large-particle samples were taken as an initial survey where the ^{230}Th activities

were likely to be relatively high. Ratios of Cd, Mn, Co, Fe, Al, and ^{232}Th to ^{230}Th are all larger in the LSF compared to the SSF (by average factors of 2.0, 1.7, 2.2, 2.1, 2.2, and 1.4, respectively). This is consistent with elevated activity of scavenged ^{230}Th on small, higher specific surface area, particles. Ratios of P and Cu concentration to ^{230}Th activity show the opposite effect, smaller ratios in the LSF than the SSF (by average factors of 0.7 and 0.8, respectively). This potentially shows the enrichment of these biogenic elements in small biological cells or the depletion of these elements in aggregates. Of the few measurements available for LSF POC/^{230}Th ratios (n = 3), there is no strong indication for significant size fractionation between POC and ^{230}Th in the LSF and SSF (Figure 6a). These measurements are challenging as deepwater particles, more enriched in ^{230}Th, are often very low in POC (and vice versa for shallow water particles). It will be valuable in future work to collect large enough particulate samples to better determine POC/^{230}Th in the LSF of marine particles.

Selected LSF/SSF comparisons can also be made for particulate element concentration to ^{228}Th activity ratios. Multiple samples of adjacent depths had to be combined in order to analyze the LSF ^{228}Th activity with reasonable counting statistics, while almost all in situ pump samples were individually analyzed for SSF ^{228}Th activity. Therefore, we compare the combined analyses of LSF ^{228}Th to SSF ^{228}Th data that were averaged over the same depth ranges for which the LSF filters were combined (Data Set S2). Because this averaging procedure introduces more uncertainty into the analysis, size fractionation trends are less clear (Figure S4). Overall, element concentration to ^{228}Th activity ratios were similar between LSF and SSF for POC, Mn, and Co; larger in LSF than SSF for Fe and Al; and larger in SSF than LSF for P, Cd, Cu, and ^{232}Th. This is similar to the size fractionation trends seen for the other Th isotopes.

3.3. Particulate Elemental Fluxes: BATS

Using equation (5), by multiplying the radionuclide fluxes plotted in Figure 3 by the element to radionuclide ratios plotted in Figures 4–6 and S4, we derive and plot the particulate element fluxes at KN204-01-10 (BATS location) as a function of depth in Figure 7. At each data point plotted, the derived radionuclide flux integrated to that depth was multiplied by the element to radionuclide ratio measured specifically at that depth. Errors were propagated for the flux estimates using the uncertainty in radionuclide activities and element concentration to radionuclide activity ratios. The SSF particulate concentration to activity ratios is used for all isotope systems since this is the size fraction among which all four isotope systems have been measured on the same samples. In section 3.2 we have shown that across the four isotope systems, fluxes based on LSF ratios compared to those based on SSF ratios will be consistently higher for Fe and Al, consistently lower for P and Cu, and for POC, Cd, Mn, and Co there were mixed results between isotope systems. For ^{234}Th-, ^{210}Po-, and ^{230}Th-based fluxes, the fluxes using LSF ratios, where available, have also been calculated and are reported in Data Set S3.

3.3.1. POC Fluxes

Measured at about 100-m depth at KN204-01-10, POC fluxes from all four radionuclide methods are (with 1 sigma uncertainties) as follows: 0.3 ± 0.6 mmol/m^2/day (^{234}Th-based), 2.8 ± 0.4 mmol/m^2/day (^{230}Th-based), 3.7 ± 0.5 mmol/m^2/day (^{228}Th-based), and 4.1 ± 0.5 mmol/m^2/day (^{210}Po-based; Figure 7a). The negligible primary production zone deficit of ^{234}Th activity seen in Figure 3a at this occupation leads to low ^{234}Th-based estimates for all elemental fluxes (Figure 7), but the fluxes derived from the other three systems are consistent with each other within 2 sigma uncertainty. The export caught in the BATS sediment trap at 150 m in late November 2011 was 1.0 mmol/m^2/day POC flux (bats.bios.edu), which is closer to the ^{234}Th-based estimated. The BATS climatological (1988–2012) POC flux during November in the 150 m trap is 2.3 ± 0.8 mmol/m^2/day (average and standard deviation of monthly means; Church et al., 2013), which is consistent with the estimates based on the longer-lived radioisotopes. This is good evidence that ^{210}Po, ^{228}Th, and ^{230}Th-based fluxes are likely capturing seasonal, annual, or longer averages of the POC flux, and the ^{234}Th flux is capturing a week-to-month-scale minimum in POC flux. These estimates are sensitive to the POC/radionuclide ratio, given the patterns seen in Figures 4 and 5. If LSF ratios are used, the POC flux based on ^{234}Th and ^{210}Po deficits is about a factor of 2 higher than with using the SSF ratios as in Figure 7. POC flux based on ^{234}Th deficits from individual station occupations at BATS, in general using LSF particulate ratios, has ranged from 0 to 7 mmol/m^2/day over 25 years of measurements (Buesseler et al., 2008; Kim & Church, 2001; Sweeney et al., 2003; Figure 7a), which nicely encompasses the longer term average fluxes estimated from the longer lived nuclides. Water column ^{234}Th-based-POC flux estimates at 100 m from the BaRFlux program, using SSF

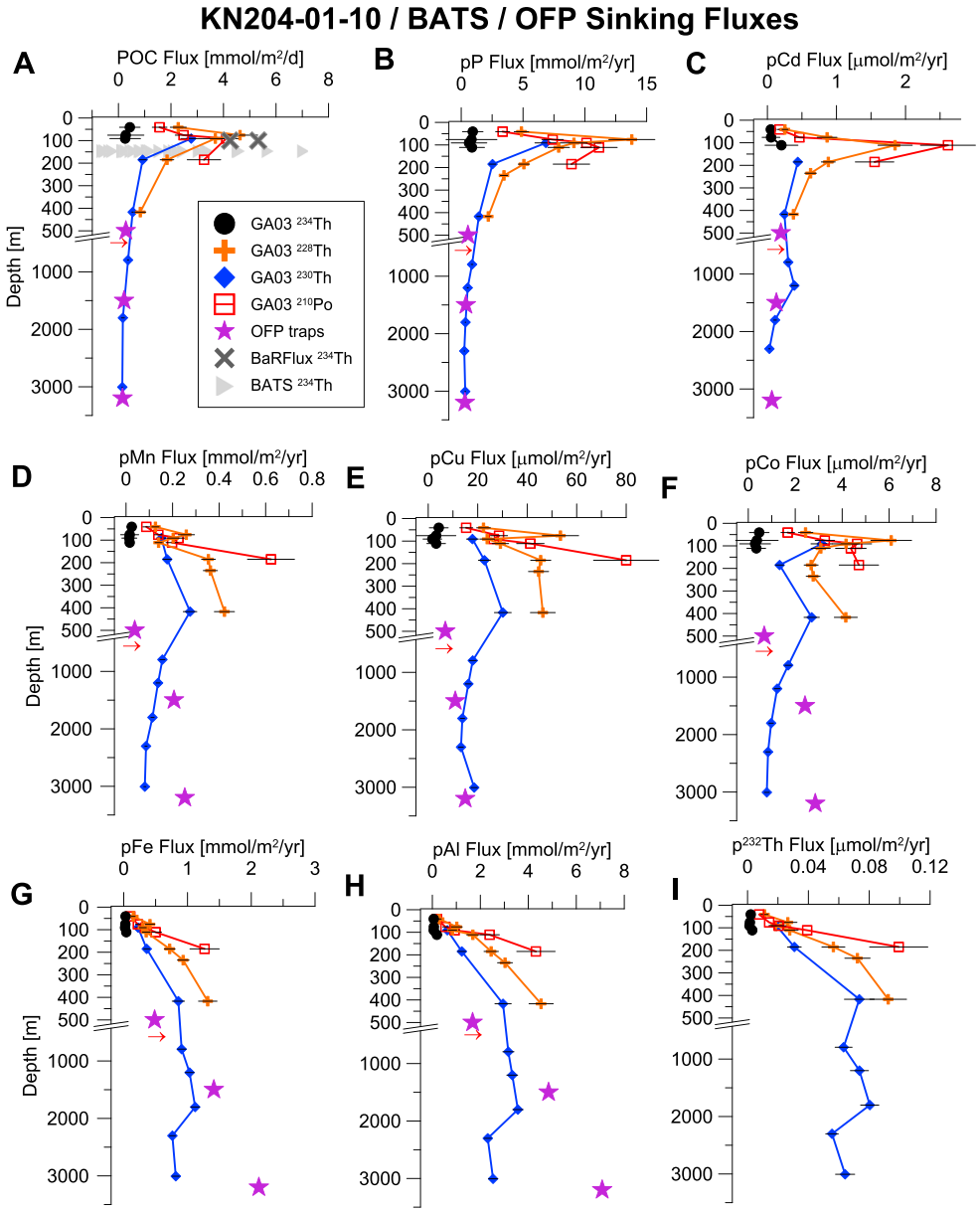

Figure 7. Sinking flux profiles as a function of integration depth in the water column at the Bermuda Atlantic Time-series (BATS) station as occupied in November 2011 on GA03. Particulate elements are denoted with a preceding *p*. Estimates based on ^{234}Th and ^{210}Po are only integrated to the base of the primary productivity zone. Fluxes based on ^{228}Th are integrated to 500 m depth, where ^{228}Th regains secular equilibrium with ^{228}Ra (see Figures 2, 3). Fluxes based on ^{230}Th are integrated to 3 km because a nepheloid layer occurs between that depth and the seafloor (~4.5-km depth). The purple stars indicate measured sediment trap fluxes from the OFP site (Huang & Conte, 2009). The red arrow at the 500-m trap data points indicates that evidence suggests this type of trap at this depth tends to undercollect (Scholten et al., 2001; Yu et al., 2001) and therefore is an underestimate of the true flux. The gray cross signs in (a) are the integrated ^{234}Th-based POC fluxes to 100 m, based on occupations of the BaRFlux site (May 2012 and June 2013). The gray triangles in (a) are ^{234}Th-based POC flux estimates over 25 years of measurements (Buesseler et al., 2008; Kim & Church, 2001; Sweeney et al., 2003) for a comparison of the historical range observed.

POC/^{234}Th ratios (1–70 µm) in May 2012 and June 2013, were 5.3 ± 1.3 and 4.3 ± 0.6 mmol/m^2/day, respectively, also well within the historical range of measurements in this region of the ocean (Figure 7a).

Below 200 m, we can compare radionuclide-based fluxes using the ^{230}Th and ^{228}Th methods with the average fluxes (2002–2005) into the moored sediment traps at the OFP site (Huang & Conte, 2009).

Note that the 500-m OFP trap may undercollect material by up to a factor of 2, as have other similar bottom-tethered conical traps shallower than 1-km depth (Scholten et al., 2001; Yu et al., 2001). Nonetheless, we can therefore use the material caught in the 500-m OFP trap data as a minimum estimate. POC fluxes from ^{230}Th and ^{228}Th activities agree well with one another between 100 and 400 m with about 1.5 mmol/m^2/day (Figure 7a), and the OFP trap at 500 m was 0.3 mmol/m^2/day. Below 1,000 m, ^{230}Th-based POC flux estimates (0.17 ± 0.06 and 0.15 ± 0.01 mmol/m^2/day at 1,800 and 3,000 m, respectively) agree notably well with the OFP trap observations at 1,500 and 3,200 m, 0.22 and 0.16 mmol/m^2/day, respectively.

3.3.2. Particulate P and Cd Fluxes

Particulate P and Cd flux profiles estimated from the KN204-01-10 data have shapes similar to the POC flux profiles, showing power law-type decay with depth (Figures 7b and 7c). One exception is a slight local maximum in ^{230}Th-based Cd flux at around 1,200-m depth that may be related to lateral transport from the North American margin (Lam et al., 2015). The overall power law shape of the profiles nonetheless suggests that particulate P and Cd are largely associated with particulate organic matter in the primary production zone and that C, P and Cd are regenerated at depth as biogenic particles are respired, potentially at different rates. The flux profiles can be fit with a power law of the form, $\text{Flux}(z) = \text{Flux}(100\text{ m}) * (z/100)^{-b}$ (Martin et al., 1987). The fitted *b* parameter is an indicator of the strength of flux attenuation with depth, which is related to remineralization rate. At KN204-01-10, using the ^{230}Th-based data between the surface and 3-km depth, the *b* values for POC, particulate P, and particulate Cd fluxes are 1.81 ± 0.07, 1.91 ± 0.06, and 1.78 ± 0.37, respectively (±1 standard error). These values are nearly indistinguishable within uncertainties.

This POC *b* value of 1.8 at BATS is relatively high compared to *b* values estimated from deep-sea moored sediment traps (0.6–2.0; Berelson, 2001; François et al., 2002) However, more recent programs using neutrally buoyant sediment traps have found higher *b* values in the oligotrophic ocean of ~1.3 at the Hawaii time series station, A Long-Term Oligotrophic Habitat Assessment (ALOHA; Buesseler et al., 2007b) and 1.6 in the northeast portion of the North Atlantic subtropical gyre (Marsay et al., 2015; see also Figure S10 where the data from Marsay et al. can be compared directly with nearby station KN204-01-20). The *b* values derived for KN204-01 stations 12 thru 22 (see Figure 1 for locations) for ^{230}Th-based POC flux (0- to 3-km depth) range from 0.8 to 1.6 (derived from Data Set S3) and support the prediction of Marsay et al. (2015) for relatively high *b* values in this range throughout the subtropical gyres.

As for the flux method comparison, ^{234}Th-based fluxes of P and Cd are again low compared to the other methods as expected from the low ^{234}Th deficit during this particular occupation. The three other radionuclide methods are all consistent with each other within about 40% in the upper 200 m. At 1,500 and 3,200 m, the ^{230}Th-based fluxes agree well with the OFP trap fluxes of about 0.5 mmol P/m^2/year and 0.1 μmol Cd/m^2/year, respectively.

3.3.3. Particulate Mn, Cu, and Co Fluxes

The flux profiles of particulate Mn, Cu, and Co (Figures 7d–7f) tend to increase with depth in the upper 500 m. This could be related to scavenging of these metals onto particles as they sink or an influence of lateral transport of particulate metals, which would be consistent with the inferred lateral supply of excess ^{234}Th to the BATS site (section 3.1). Aside from the expected low ^{234}Th-based results, the other three methods agree reasonably well in the upper 150 m for these elements. For particulate Co, there is some attenuation in flux with depth between 100 and 200 m (in ^{228}Th- and ^{230}Th-based estimates) possibly indicating the influence of biogenic particulate Co regeneration. In support of this idea, total particulate Co was determined to be about 60% biogenic (i.e., found in phytoplankton cells) in the euphotic zone of KN204-01-10 (Twining, Rauschenberg, Morton, & Vogt, 2015). Indeed, Co was correlated with P in the upper 400 m, indicating biogenic behavior, but with Mn below 400 m, illustrating scavenging behavior and its classification as a *hybrid-type* metal (Saito et al., 2017). The ^{210}Po-based estimates at 200-m depth and the ^{228}Th-based estimates between 200 and 500 m are higher than the ^{230}Th-based estimates by up to a factor of 3. Indeed, fluxes derived from ^{228}Th and ^{210}Po deficits were systematically higher than those from derived from ^{230}Th for almost all elements for this station and the other stations analyzed (section 3.3.5; supporting information). This may be due to the fact that the parent isotopes of these pairs (^{228}Ra and ^{210}Pb) are supplied to the ocean without significant accompanying amounts of their daughters, thereby creating an initial disequilibrium that is unrelated to scavenging. This effect is discussed in detail in section 4.1.

Between 500 and 2,500 m, particulate fluxes of Mn, Cu, and Co all decrease, possibly indicating deep regeneration processes or lateral input of these metals at shallower depths (200–500 m). This is in contrast to the findings of one study that reconstructed trace element fluxes using neutrally buoyant sediment traps at 100-, 300-, and 500-m depth from Station ALOHA in the North Pacific subtropical gyre (Lamborg et al., 2008). These authors found relatively constant flux within 100- to 500-m depth for Mn, Co, Cu, Fe, Al, and Sc. Boyd et al. (2017) highlighted this result as these elements being a *lithogenic throughput* of mineral dust particles. The results presented here, however, argue more in favor a mixture of authigenic, lithogenic, and biogenic particulate fractions being important for these elements.

The ^{230}Th-based fluxes of these elements are within about 50% of the fluxes observed in the 1,500- and 3,200-m OFP traps. Below 3,000 m the flux profiles of these elements clearly show the influence of the extended nepheloid layer that has been observed at BATS (Gardner et al., 2018; Lam et al., 2015; Sherrell & Boyle, 1992). This layer of resuspended sediments extends about 1 km above the seafloor (to about 3500-m depth). Extended benthic nepheloid layers can be found over much of the western Atlantic margin (Biscaye & Eittreim, 1977; Gardner et al., 2018).

3.3.4. Particulate Fe, Al, and ^{232}Th Fluxes

Flux profiles of the lithogenic elements, Fe, Al, and ^{232}Th, also increase with depth from the surface to 500 m (Figures 7g–7i), and there is fair agreement between methods on the magnitudes of these fluxes. From 500 to 2,000 m, the fluxes of these elements continue to increase. This could be the result of continued scavenging of the dissolved metals onto particles or lateral advection of suspended clays and other lithogenic grains by deepwater currents originating from the western Atlantic margin (Jickells et al., 1987). The latter process has been proposed to explain the increasing fluxes of Fe and Al in the OFP trap profile (Huang & Conte, 2009). Below 3.5-km depth, fluxes of Fe, Al, and ^{232}Th are clearly influenced by the nepheloid layer, and thus, the fluxes derived for these depths cannot be considered true sinking fluxes.

3.3.5. Flux Profiles From Other GA03 Stations

Many of the same conclusions can be made for the four method comparison of flux estimates at the six other stations with available data from GA03 (starred stations in Figure 1). The flux comparisons for these other stations are presented in Figures S5–S10. In contrast to the results from KN204-01-10, at other stations, ^{234}Th-based fluxes are in better agreement with the other methods, likely indicating that at the time of sampling the recent export flux was closer to a climatological mean. In particular, at station KN199-04-09 there are also existing trace element sediment trap results from a nearby sediment trap (KS93 in Figure 1; Kremling & Streu, 1993) that compare well with the radionuclide based fluxes (Figure S6).

4. Discussion

4.1. Basin-Scale View of Upper Ocean Element Export and Possible Margin-to-Gyre Anomalies

In Figure 8, we have compiled flux measurements from GA03 stations, across the same section as in Figure 2, exported to the depth at the base of the PPZ (Owens et al., 2015) for all radionuclide methods available at each location (using only SSF particulate ratios). We show here only POC, particulate Co, and particulate Fe fluxes as representative of the spectrum of elemental behaviors, from biogenic to lithogenic. For the most part, when results from multiple methods are available, they agree well (roughly within a factor of 2) given all the uncertainties associated with timescale integration, circulation effects, and differential scavenging behavior. These three and all other elements considered show elevated particulate fluxes near the North American and West African margins on either ends of the transect and reduced particulate fluxes in the subtropical gyre stations (longitudes 56.8–29.4°W; Figure 8).

Two possible systematic differences can be seen in this comparison. First, the ^{210}Po method may be overestimating flux in the subtropical gyre stations, generally more so than the margin stations. The fact that there is a larger ^{210}Po deficit in the oligotrophic ocean than would be expected based on particle flux alone has been hypothesized to be related to a greater transfer of Po to higher trophic levels in the ocean interior versus the margin (Kim, 2001). Another possibility is that low ^{210}Po water from highly scavenged margin areas, if advected into the gyre, could contribute to high deficits in the gyre. This possibility is best addressed with the use of a general circulation model as we do not have adequate current speed information from our sampling to know if such advection occured. Instead, we offer a third alternative hypothesis for this discrepancy based on the distribution of the parent isotope ^{210}Pb in GA03. The atmospheric source of ^{210}Pb causes

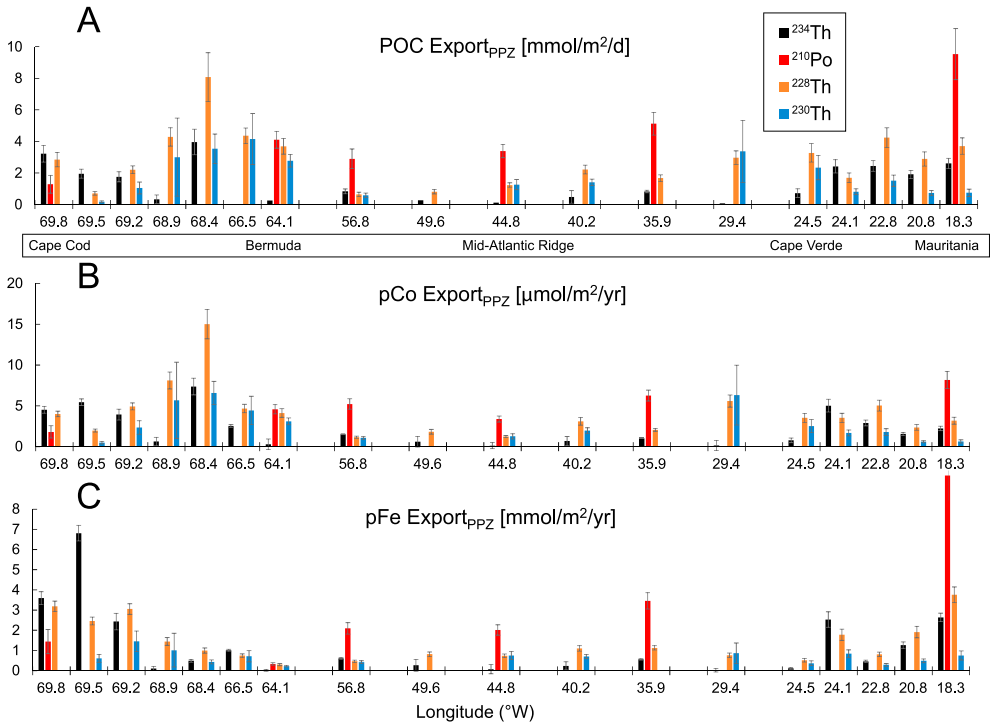

Figure 8. Fluxes of particulate organic carbon, Co, and Fe derived for the base of the primary productivity zone, at which fluorescence drops to 10% of its surface value, from the four radionuclide methods across the North Atlantic. Fluxes based on ^{234}Th are in black, ^{210}Po in red, ^{228}Th in orange, and ^{230}Th in blue.

seawater ^{210}Pb/^{226}Ra activity ratios to be in excess of 1 (secular equilibrium), as the aerosols have a high ^{210}Pb/^{226}Ra ratio. The source of in situ decay, on the other hand, would result in ^{210}Pb/^{226}Ra ratios close to 1. The total ^{210}Pb/^{226}Ra activity ratio in the upper 500 m of the water column at the North American margin (KN204-01-01) is between 1 and 1.2, while in the subtropical gyre stations this ratio is between 2 and 3, indicating a much larger fraction of the ^{210}Pb is sourced from atmospheric deposition in the ocean interior (Figure S11; also discussed by Rigaud et al., 2015). This is significant in that aerosols have very low ^{210}Po/^{210}Pb ratios ($<$0.1; Baskaran, 2011). The assumed residence time of ^{210}Pb in surface waters of 2 years (equivalent to 5.3 half-lives of ^{210}Po) should be sufficient time for an initial ^{210}Po/^{210}Pb activity ratio of 0.1 to reach near secular equilibrium (~0.97). However, since ^{210}Po is constantly being scavenged, perhaps secular equilibrium should not be the starting assumption for this radionuclide pair in seawater. In other words, atmospheric deposition adds a source of ^{210}Pb that is already depleted with respect to its daughter product, and therefore, an apparent ^{210}Po deficit is created, even if there were no particle export of Po. Furthermore, there is a very high ^{210}Pb/^{226}Ra activity ratio (2.6) in the upper 30 m of the Mauritanian margin (KN199-04-09), potentially because of the large Saharan dust deposition at this site (Anderson et al., 2016), which also leads to anomalous high flux estimates here (Figure 8).

The second, more subtle, but systematic difference we notice is ^{228}Th-based fluxes being larger than other fluxes to a greater extent in the margins compared to the gyre (opposite of the ^{210}Po effect; Figure 8). The BATS results discussed in section 3 appear to be somewhere near the boundary between the *margin* and *gyre* stations with respect to these effects. In this case, the geographical source function of the parent isotope ^{228}Ra may also impact the derived fluxes. The addition of ^{228}Ra to the ocean occurs to the greatest extent near ocean margins (Charette et al., 2015) from coastal sources, which are likely depleted in ^{228}Th with respect its parent. High particle fluxes in these coastal regions also strongly scavenge ^{228}Th (Broecker et al., 1973; Rutgers van der Loeff et al., 2012). This would result in ^{228}Th deficits that are *too high*. In other words, the deficits in the margin are due not only to local scavenging but also preexisting deficits from distal ^{228}Ra supply and ^{228}Th removal near the coast. The effect results in local fluxes that are overestimates in the margin stations. Once in the gyre, enough time has passed to allow the ^{228}Th to grow in and its deficit with

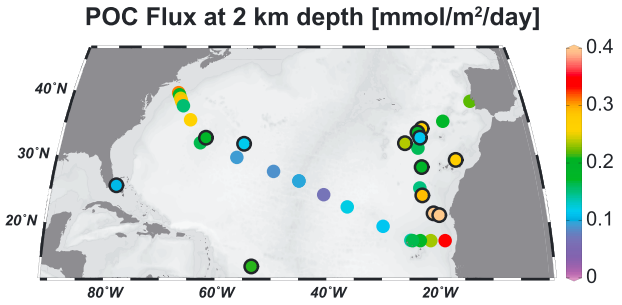

Figure 9. Comparison of particulate organic carbon fluxes determined at 2-km water depth by the particulate ^{230}Th method presented here in colored circles and from the compilation of deep sediment trap data by Honjo et al. (2008) in colored circles with black outlines.

respect to ^{228}Ra is due mostly to local scavenging, thus accounting for the better consistency between fluxes derived from ^{228}Th and from ^{230}Th in the gyre.

4.2. Assessment of POC Flux Into the Deep Sea in the North Atlantic

As discussed by Honjo et al. (2008), the biological pump is a complex, grand process that transports carbon from the atmosphere to the deep sea through sinking particles. The biological pump regulates Earth's climate to the extent that the ocean sequesters the greenhouse gas CO_2 from the atmosphere. Owens et al. (2015), using GA03 ^{234}Th data, calculated in detail the POC flux associated with the *upper* part of this biological pump, that is, from the surface ocean to below the primary production zone, across the Atlantic. The ^{210}Po-based POC fluxes reported here provide additional constraints on this upper ocean flux. The deep flux profiles, which can be gleaned from the longer-lived ^{228}Th and ^{230}Th, provide new and important constraints on particle remineralization rates across the thermocline, the quantification of which has been a target of recent research (Marsay et al., 2015; Weber et al., 2016). Additionally, the ^{230}Th-based flux profiles can be extended to the mesopelagic/bathypelagic (m/b) boundary, at roughly 2-km depth. Honjo et al. (2008) point out that flux across the *m/b* boundary leads to storage of carbon in the deep sea much longer (centuries to millennia; e.g., Primeau, 2005) than in the upper ocean.

In Figure 9, we compare the ^{230}Th-based POC fluxes at 2 km from the GA03 section with the sediment trap compilation of Honjo et al. (2008), who reported all available, annually resolved deep sediment trap POC fluxes, normalized to 2-km depth. The sediment trap compilation contains sites in the GA03 region characterizing the oligotrophic Sargasso Sea in the west of the subtropical gyre and the more biologically productive eastern margin of the subtropical gyre. In the Sargasso Sea, both deep sediment trap and ^{230}Th-based estimates of POC flux are around 0.1–0.2 mmol C/m^2/day. In the eastern North Atlantic, highest POC fluxes are seen in the upwelling area off of Mauritania, in both trap and ^{230}Th results, exceeding 0.4 mmol C/m^2/day. All along the eastern edge of the subtropical gyre, the offshore area between Portugal and Morocco, the sediment trap compilation and the GA03 ^{230}Th estimates also converge on about 0.2–0.3 mmol C/m^2/day. The agreement between these two independent methods is very encouraging and helps to validate the use of water column particulate-based ^{230}Th fluxes for broader questions.

The GA03 ^{230}Th-based deep POC fluxes add considerable detail to the known deep marine carbon cycle, constraining the low fluxes all across the oligotrophic gyre from Bermuda to Cape Verde, and showing elevated fluxes again offshore of the North American margin. When the GEOTRACES program is complete, it will constrain a much wider swath of the global ocean (Anderson et al., 2014). Based on the work presented here, analysis of particulate ^{230}Th from in situ pump sampling will be invaluable for constraining the deep portion of the global biological pump.

4.3. Tools to Investigate Trace Element Internal Cycling

The particulate element fluxes presented here will be invaluable targets for biogeochemical modeling of these elements. In particular, the depth profile of fluxes is very novel for the elements studied here. The shape of these profiles allows testing of the impacts of relative rates of particle regeneration, particle sinking rates, scavenging rates, and other processes, in different environments across the GA03 transect. For upper ocean processes, the range in fluxes constrained by the ^{234}Th, ^{210}Po, and ^{228}Th methods, measured at high depth resolution in the upper water column, will be the most useful constraints. Using the deep ^{230}Th fluxes, questions about the longer term, basin-wide cycling of the elements can be addressed. A full investigation of any of these topics is beyond the scope of this study, but they are all worthy of future coupled physical-biogeochemical general circulation modeling.

5. Conclusions

This study has been a synthesis of unparalleled comprehensiveness using GEOTRACES radionuclide and trace element data that to our knowledge has never been done before with four radionuclide systems all measured

on the same samples. In the upper 500 m of the water column, particulate fluxes of organic carbon and a spectrum of trace elements can be derived using all four different radionuclide pairs. It is clear that ^{234}Th fluxes are tracking recent (weekly-monthly) particle dynamics in the primary production zone, whereas fluxes of the longer lived ^{228}Th and ^{230}Th indicate annual or longer integration times of particle flux. Fluxes based on ^{210}Po deficits in the interior ocean were often higher than those based on the other radionuclide methods, potentially related to the mode of introduction of its parent ^{210}Pb to the surface ocean. Throughout the water column below 500 m, particulate ^{230}Th profiles provide robust estimates, within roughly a factor of 2, of thermocline and deep particulate fluxes, validated in this study by proximal deep sediment traps, both for organic carbon and the trace elements considered. In sum, the GA03 particulate flux data set offers a rich target for coupled physical-biogeochemical general circulation modeling of trace elements. The GEOTRACES program was designed to allow for synthesis efforts of this sort. Without the collaboration of multiple laboratories within a coordinated program, the constraints provided in this study would not have been possible. Future research programs will similarly benefit by coordinating multiple complementary observations to derive products that are not directly measurable.

Acknowledgments

This study grew out of a synthesis workshop at the Lamont-Doherty Earth Observatory of Columbia University in August 2016. This workshop was sponsored by the U.S. GEOTRACES Project Office (NSF 1536294) and the Ocean Carbon and Biogeochemistry (OCP) Project Office (NSF 1558412 and NASA NNX17AB17G). The U.S. National Science Foundation supported all of the analytical work on GA03. Kuanbo Zhou measured ^{228}Th in the large size class particles (NSF 0925158 to WHOI). NSF 1061128 to Stony Brook University supported the BaRFlux project, for which Chistina Heilbrun is acknowledged for laboratory and field work. The lead author acknowledges support from a start-up grant from the University of Southern Mississippi. Two anonymous reviewers are thanked for their constructive comments. All GEOTRACES GA03 data used in this study are accessible through the Biological and Chemical Oceanography Data Management Office (http://data.bco-dmo.org/jg/dir/BCO/GEOTRACES/NorthAtlanticTransect/), and derived parameters are reported in the supporting information.

References

Abramson, L., Lee, C., Liu, Z., Wakeham, S. G., & Szlosek, J. (2010). Exchange between suspended and sinking particles in the northwest Mediterranean as inferred from the organic composition of in situ pump and sediment trap samples. *Limnology and Oceanography*, *55*(2), 725–739. https://doi.org/10.4319/lo.2009.55.2.0725

Andersen, M. B., Stirling, C. H., & Zimmermann, B. (2010). Precise determination of the open ocean ^{234}U/^{238}U composition. *Geochemistry, Geophysics, Geosystems*, *11*, Q12003. https://doi.org/10.1029/2010GC003318

Anderson, R. F., Cheng, H., Edwards, R. L., Fleisher, M. Q., Hayes, C. T., Huang, K., et al. (2016). How well can we quantify dust deposition to the ocean? *Philosophical Transactions of the Royal Society A*, *374*(2081), 20150285. https://doi.org/10.1098/rsta.2015.0285

Anderson, R. F., Mawji, E., Cutter, G. A., Measures, C. I., & Jeandel, C. (2014). GEOTRACES: Changing the way we explore ocean chemistry. *Oceanography*, *27*(1), 50–61. https://doi.org/10.5670/oceanog.2014.07

Auro, M. E., Robinson, L. F., Burke, A., Bradtmiller, L. I., Fleisher, M. Q., & Anderson, R. F. (2012). Improvements to 232-thorium, 230-thorium, and 231-protactinium analysis in seawater arising from GEOTRACES intercalibration. *Limnology and Oceanography: Methods*, *10*(7), 464–474. https://doi.org/10.4319/lom.2012.10.464

Bacon, M. P., & Anderson, R. F. (1982). Distribution of thorium isotopes between dissolved and particulate forms in the deep sea. *Journal of Geophysical Research*, *87*(C3), 2045–2056. https://doi.org/10.1029/JC087iC03p02045

Bacon, M. P., Cochran, J. K., Hirschberg, D., Fleer, A. P., & Hammar, T. R. (1996). Export flux of carbon at the equator during the EqPac time-series cruises estimated from ^{234}Th measurements. *Deep Sea Research, Part II*, *43*(4-6), 1133–1153. https://doi.org/10.1016/0967-0645(96)00016-1

Bacon, M. P., Huh, C.-A., Fleer, A. P., & Deuser, W. G. (1985). Seasonality in the flux of natural radionuclides and plutonium in the deep Sargasso Sea. *Deep Sea Research*, *32*(3), 273–286. https://doi.org/10.1016/0198-0149(85)90079-2

Bacon, M. P., Spencer, D. W., & Brewer, P. G. (1976). ^{210}Pb/^{226}Ra and ^{210}Po/^{210}Pb disequilibria in seawater and suspended particulate matter. *Earth and Planetary Science Letters*, *32*(2), 277–296. https://doi.org/10.1016/0012-821X(76)90068-6

Baskaran, M. (2011). Po-210 and Pb-210 as atmospheric tracers and global atmospheric Pb-210 fallout: A review. *Journal of Environmental Radioactivity*, *102*(5), 500–513. https://doi.org/10.1016/j.jenvrad.2010.10.007

Benitez-Nelson, C., Buesseler, K. O., Karl, D. M., & Andrews, J. (2001). A time-series study of particulate matter export in the North Pacific Subtropical Gyre based on ^{234}Th:^{238}U disequilibrium. *Deep Sea Research, Part I*, *48*(12), 2595–2611. https://doi.org/10.1016/S0967-0637(01)00032-2

Berelson, W. (2001). The flux of particulate organic carbon into the ocean interior: A comparison of four U.S. JGOFS regional studies. *Oceanography*, *14*(4), 59–67. https://doi.org/10.5670/oceanog.2001.07

Bhat, S. G., Krishnaswami, S., Lal, D., Rama, & Moore, W. S. (1969). ^{234}Th/^{238}U ratios in the ocean. *Earth and Planetary Science Letters*, *5*, 483–491. https://doi.org/10.1016/S0012-821X(68)80083-4

Biscaye, P. E., & Eittreim, S. L. (1977). Suspended particulate loads and transports in the nepheloid layer of the abyssal Atlantic Ocean. *Marine Geology*, *23*(1-2), 155–172. https://doi.org/10.1016/0025-3227(77)90087-1

Bishop, J. K. B., Lam, P. J., & Wood, T. J. (2012). Getting good particles: Accurate sampling of particles by large volume in-situ filtration. *Limnology and Oceanography: Methods*, *10*(9), 681–710. https://doi.org/10.4319/lom.2012.10.681

Black, E. E., Buesseler, K. O., Pike, S. M., & Lam, P. J. (2018). ^{234}Th as a tracer of particulate export and remineralization in the southeastern tropical Pacific. *Marine Chemistry*, *201*, 35–50. https://doi.org/10.1016/j.marchem.2017.06.009

Bory, A., Jeandel, C., Leblond, N., Vangriesheim, A., Khripounoff, A., Beaufort, L., et al. (2001). Downward particle fluxes within different productivity regimes off the Mauritanian upwelling zone (EUMELI program). *Deep Sea Research, Part I*, *48*(10), 2251–2282. https://doi.org/10.1016/S0967-0637(01)00010-3

Boyd, P. W., Ellwood, M. J., Tagliabue, A., & Twining, B. S. (2017). Biotic and abiotic retention, recycling and remineralization of metals in the ocean. *Nature Geoscience*, *10*(3), 167–173. https://doi.org/10.1038/ngeo2876

Broecker, W. S., Kaufman, A., & Trier, R. M. (1973). The residence time of thorium in surface sea water and its implications regarding the rate of reactive pollutants. *Earth and Planetary Science Letters*, *20*(1), 35–44. https://doi.org/10.1016/0012-821X(73)90137-4

Buesseler, K., Bacon, M. P., Cochran, J. K., & Livingston, H. D. (1992). Carbon and nitrogen export during the JGOFS North Atlantic Bloom Experiment estimated from ^{234}Th:^{238}U disequilibria. *Deep Sea Research*, *39*(7-8), 1115–1137. https://doi.org/10.1016/0198-0149(92)90060-7

Buesseler, K., Ball, L., Andrews, J., Benitez-Nelson, C., Belastock, R., Chai, F., & Chao, Y. (1998). Upper Ocean export of particulate organic carbon in the Arabian Sea derived from thorium-234. *Deep Sea Research, Part II*, *45*(10-11), 2461–2487. https://doi.org/10.1016/S0967-0645(98)80022-2

Buesseler, K. O., Andrews, J. A., Hartman, M. C., Belastock, R., & Chai, F. (1995). Regional estimates of the export flux of particulate organic carbon derived from thorium-234 during the JGOFS EqPac program. *Deep Sea Research, Part II*, *42*(2-3), 777–804. https://doi.org/10.1016/0967-0645(95)00043-P

Buesseler, K. O., Antia, A. N., Chen, M., Fowler, S. W., Gardner, W. D., Gustafsson, O., et al. (2007b). An assessment of the use of sediment traps for estimating upper ocean particle fluxes. *Journal of Marine Research*, *65*(3), 345–416. https://doi.org/10.1357/002224007781567621

Buesseler, K. O., Benitez-Nelson, C., Rutgers van der Loeff, M., Andrews, J., Ball, L., Crossin, G., & Charette, M. A. (2001). An intercomparison of small- and large-volume techniques for thorium-234 in seawater. *Marine Chemistry*, *74*(1), 15–28. https://doi.org/10.1016/S0304-4203(00)00092-X

Buesseler, K. O., Benitez-Nelson, C. R., Moran, S. B., Burd, A., & Charette, M. (2006). An assessment of particulate organic carbon to thorium-234 ratios in the ocean and their impact on the application of ^{234}Th as a POC flux proxy. *Marine Chemistry*, *100*(3-4), 213–233. https://doi.org/10.1016/j.marchem.2005.10.013

Buesseler, K. O., Lamborg, C., Cai, P., Escoube, R., Johnson, R., Pike, S., et al. (2008). Particle fluxes associated with mesoscale eddies in the Sargasso Sea. *Deep Sea Research, Part II*, *55*(10-13), 1426–1444. https://doi.org/10.1016/j.dsr2.2008.02.007

Buesseler, K. O., Lamborg, C. H., Boyd, P. W., Lam, P. J., Trull, T. W., Bidigare, R. R., et al. (2007a). Revisiting carbon flux through the ocean's twilight zone. *Science*, *316*(5824), 567–570. https://doi.org/10.1126/science.1137959

Buesseler, K. O., Pike, S., Maiti, K., Lamborg, C. H., Siegel, D. A., & Trull, T. W. (2009). Thorium-234 as a tracer of spatial, temporal and vertical variability in particle flux in the North Pacific. *Deep Sea Research, Part I*, *56*(7), 1143–1167. https://doi.org/10.1016/j.dsr.2009.04.001.

Charette, M. A., Morris, P. J., Henderson, P. B., & Moore, W. S. (2015). Radium isotope distributions during the US GEOTRACES North Atlantic cruises. *Marine Chemistry*, *177*, 184–195. https://doi.org/10.1016/j.marchem.2015.01.001

Church, M. J., Lomas, M. W., & Muller-Karger, F. (2013). Sea change: Charting the course for biogeochemical ocean time-series research in a new millennium. *Deep Sea Research, Part II*, *93*, 2–15. https://doi.org/10.1016/j.dsr2.2013.01.035

Church, T., Rigaud, S., Baskaran, M., Kumar, A., Friedrich, J., Masque, P., et al. (2012). Intercalibration studies of ^{210}Po and ^{210}Pb in dissolved and particulate seawater samples. *Limnology and Oceanography: Methods*, *10*(10), 776–789. https://doi.org/10.4319/lom.2012.10.776

Coale, K. H., & Bruland, K. W. (1987). Oceanic stratified euphotic zone as elucidated by ^{234}Th:^{238}U disequilibria. *Limnology and Oceanography*, *32*(1), 189–200. https://doi.org/10.4319/lo.1987.32.1.0189

Cochran, J. K., & Masqué, P. (2003). Short-lived U/Th series radionuclides in the ocean: Tracers for scavenging rates, export fluxes and particle dynamics. *Rev. Mineral. Geochemistry*, *52*(1), 461–492. https://doi.org/10.2113/0520461

Collier, R., & Edmond, J. (1984). The trace element geochemistry of marine biogenic particulate matter. *Progress in Oceanography*, *13*(2), 113–199. https://doi.org/10.1016/0079-6611(84)90008-9

Fisher, N. S., Burns, K. A., Cherry, R. D., & Heyraud, M. (1983). Accumulation and cellular distribution of ^{241}Am, ^{210}Po, and ^{210}Pb in two marine algae. *Marine Ecology Progress Series*, *11*, 233–237. https://doi.org/10.3354/meps011233

François, R., Frank, M., Rutgers van der Loeff, M. M., & Bacon, M. P. (2004). Th normalization: An essential tool for interpreting sedimentary fluxes during the late Quaternary. *Paleoceanography*, *19*, PA1018. https://doi.org/10.1029/2003PA000939

François, R., Honjo, S., Krishfield, R., & Manganini, S. (2002). Factors controlling the flux of organic carbon to the bathypelagic zone of the ocean. *Global Biogeochemical Cycles*, *16*(4), 1087. https://doi.org/10.1029/2001GB001722

Gardner, W. D., Biscaye, P. E., & Richardson, M. J. (1997). A sediment trap experiment in the Vema Channel to evaluate the effect of horizontal particle fluxes on measured vertical fluxes. *Journal of Marine Research*, *55*(5), 995–1028. https://doi.org/10.1357/0022240973224139

Gardner, W. D., Richardson, M. J., & Mishonov, A. V. (2018). Global assessment of benthic nepheloid layers and linkage with upper ocean dynamics. *Earth and Planetary Science Letters*, *482*, 126–134. https://doi.org/10.1016/j.epsl.2017.11.008

Hansell, D. A., & Newton, J. A. (1994). Design and evaluation of a swimmer segregating particle interceptor trap. *Limnology and Oceanography*, *39*(6), 1487–1495. https://doi.org/10.4319/lo.1994.39.6.1487

Hayes, C. T., Anderson, R. F., Fleisher, M. Q., Huang, K. F., Robinson, L. F., et al. (2015b). ^{230}Th and ^{231}Pa on GEOTRACES GA03, the U.S. GEOTRACES North Atlantic transect, and implications for modern and paleoceanographic chemical fluxes. *Deep Sea Research, Part II*, *116*, 29–41. https://doi.org/10.1016/j.dsr2.2014.07.007

Hayes, C. T., Anderson, R. F., Fleisher, M. Q., Vivancos, S. M., Lam, P. J., Ohnemus, D. C., et al. (2015a). Intensity of Th and Pa scavenging partitioned by particle chemistry in the North Atlantic Ocean. *Marine Chemistry*, *170*, 49–60. https://doi.org/10.1016/j.marchem.2015.01.006

Helmke, P., Romero, O., & Fischer, G. (2005). Northwest African upwelling and its effect on offshore organic carbon export to the deep sea. *Global Biogeochemical Cycles*, *19*, GB4015. https://doi.org/10.1029/2004GB002265

Henderson, G. M., Heinze, C., Anderson, R. F., & Winguth, A. M. E. (1999). Global distribution of the 230Th flux to ocean sediments constrained by GCM modelling. *Deep Sea Research, Part I*, *46*(11), 1861–1893. https://doi.org/10.1016/S0967-0637(99)00030-8

Hirose, K. (2006). A new method to determine depth-dependent carbon export fluxes using vertical ^{230}Th profiles. *Geophysical Research Letters*, *33*, L05609. https://doi.org/10.1029/2005GL025129

Hong, G. H., Baskaran, M., Church, T. M., & Conte, M. (2013). Scavenging, cycling and removal fluxes of ^{210}Po and ^{210}Pb at the Bermuda time-series study site. *Deep Sea Research, Part II*, *93*, 108–118. https://doi.org/10.1016/j.dsr2.2013.01.005

Honjo, S., Manganini, S. J., Krishfield, R. A., & Francois, R. (2008). Particulate organic carbon fluxes to the ocean interior and factors controlling the biological pump: A synthesis of global sediment trap programs since 1983. *Progress in Oceanography*, *76*(3), 217–285. https://doi.org/10.1016/j.pocean.2007.11.003

Huang, S., & Conte, M. H. (2009). Source/process apportionment of major and trace elements in sinking particles in the Sargasso sea. *Geochimica et Cosmochimica Acta*, *73*(1), 65–90. https://doi.org/10.1016/j.gca.2008.08.023

Jickells, T. D., Church, T. M., & Deuser, W. G. (1987). A comparison of atmospheric inputs and deep-ocean particle fluxes for the Sargasso Sea. *Global Biogeochemical Cycles*, *1*(2), 117–130. https://doi.org/10.1029/GB001i002p00117

Kim, G. (2001). Large deficiency of polonium in the oligotrophic ocean's interior. *Earth and Planetary Science Letters*, *192*(1), 15–21. https://doi.org/10.1016/S0012-821X(01)00431-9

Kim, G., & Church, T. M. (2001). Seasonal biogeochemical fluxes of ^{234}Th and ^{210}Po in the upper Sargasso Sea: Influence from atmospheric iron deposition. *Global Biogeochemical Cycles*, *15*(3), 651–661. https://doi.org/10.1029/2000GB001313

Kremling, K., & Streu, P. (1993). Saharan dust influenced trace element fluxes in deep North Atlantic subtropical waters. *Deep Sea Research, Part I*, *40*(6), 1155–1168. https://doi.org/10.1016/0967-0637(93)90131-L

Ku, T. L., Knauss, K. G., & Mathieu, G. G. (1977). Uranium in open ocean: Concentration and isotopic composition. *Deep Sea Research*, *24*(11), 1005–1017. https://doi.org/10.1016/0146-6291(77)90571-9

Lam, P. J., Ohnemus, D. C., & Auro, M. E. (2015). Size-fractionated major particle composition and concentrations from the US GEOTRACES North Atlantic Zonal Transect. *Deep Sea Research, Part II*, *116*, 303–320. https://doi.org/10.1016/j.dsr2.2014.11.020

Lamborg, C. H., Buesseler, K. O., & Lam, P. J. (2008). Sinking fluxes of minor and trace elements in the North Pacific Ocean measured during the VERTIGO program. *Deep Sea Research, Part II*, *55*(14-15), 1564–1577. https://doi.org/10.1016/j.dsr2.2008.04.012

Lepore, K., & Moran, S. B. (2007). Seasonal changes in thorium scavenging and particle aggregation in the western Arctic Ocean. *Deep Sea Research, Part I*, *54*(6), 919–938. https://doi.org/10.1016/j.dsr.2007.03.001

Lerner, P., Marchal, O., Lam, P. J., Anderson, R. F., Buesseler, K., Charette, M. A., et al. (2016). Testing models of thorium and particle cycling in the ocean using data from station GT11-22 of the U.S. GEOTRACES North Atlantic Section. *Deep Sea Research*, *118*(118), 101. https://doi.org/10.1016/j.dsr.2016.09.001

Lerner, P., Marchal, O., Lam, P. J., Buesseler, K., & Charette, M. (2017). Kinetics of thorium and particle cycling along the U.S. GEOTRACES North Atlantic Transect. *Deep Sea Research, Part I*, *125*, 106–128. https://doi.org/10.1016/j.dsr.2017.05.003

Li, Y.-H., Feely, H. W., & Toggweiler, J. R. (1980). ^{228}Ra and ^{228}Th concentrations in GEOSECS Atlantic surface waters. *Deep Sea Research*, *27*(7), 545–555. https://doi.org/10.1016/0198-0149(80)90039-4

Luo, S., Ku, T. L., Kusakabe, M., Bishop, J. K., & Yang, Y. L. (1995). Tracing particle cycling in the upper ocean with ^{230}Th and ^{228}Th: An investigation in the equatorial Pacific along 140°W. *Deep Sea Research, Part II*, *42*(2-3), 805–829. https://doi.org/10.1016/0967-0645(95)00019-M

Maiti, K., Charette, M. A., Buesseler, K. O., Zhou, K., Henderso, P., Moore, W. S., et al. (2015). Determination of particulate and dissolved ^{228}Th in seawater using a delayed coincidence counter. *Marine Chemistry*, *177*, 196–202. https://doi.org/10.1016/j.marchem.2014.12.001

Maiti, K., Nelson, C. R. B., & Buesseler, K. O. (2010). Insights into particle formation and remineralization using the short-lived radionuclide, Thoruim-234. *Geophysical Research Letters*, *37*, L15608. https://doi.org/10.1029/2010GL044063

Marsay, C. M., Sanders, R. J., Henson, S. A., Pabortsava, K., Achterberg, E. P., & Lampitt, R. S. (2015). Attenuation of sinking particulate organic carbon flux through the mesopelagic ocean. *Proceedings of the National Academy of Sciences of the United States of America*, *112*(4), 1089–1094. https://doi.org/10.1073/pnas.1415311112

Martin, J. H., Knauer, G. A., Karl, D. M., & Broenkow, W. W. (1987). VERTEX: Carbon cycling in the northeast Pacific. *Deep Sea Research*, *34*(2), 267–285. https://doi.org/10.1016/0198-0149(87)90086-0

Moore, H. E., Poet, S. E., Martell, E. A., & Wilkening, M. H. (1974). Origin of ^{222}Rn and its long-lived daughters in air over Hawaii. *Journal of Geophysical Research*, *79*(33), 5019–5024. https://doi.org/10.1029/JC079i033p05019

Moore, W. S. (1969a). Measurement of ^{228}Ra and ^{228}Th in sea water. *Journal of Geophysical Research*, *74*(2), 694–704. https://doi.org/10.1029/JB074i002p00694

Moore, W. S. (1969b). Oceanic concentrations of ^{228}Radium. *Earth and Planetary Science Letters*, *6*(6), 437–446. https://doi.org/10.1016/0012-821X(69)90113-7

Moore, W. S., & Sackett, W. M. (1964). Uranium and thorium series inequilibrium in sea water. *Journal of Geophysical Research*, *69*(24), 5401–5405. https://doi.org/10.1029/JZ069i024p05401

Moore, W. S., Sarmiento, J. L., & Key, R. M. (2008). Submarine groundwater discharge revealed by ^{228}Ra distribution in the upper Atlantic Ocean. *Nature Geoscience*, *1*(5), 309–311. https://doi.org/10.1038/ngeo183

Murray, J. W., Paul, B., Dunne, J. P., & Chapin, T. (2005). ^{234}Th, ^{210}Pb, ^{210}Po and stable Pb in the central equatorial Pacific: Tracers for particle cycling. *Deep Sea Research, Part I*, *52*(11), 2109–2139. https://doi.org/10.1016/j.dsr.2005.06.016

Murray, J. W., Young, J., Newton, J., Dunne, J., Chapin, T., Paul, B., & McCarthy, J. J. (1996). Export flux of particulate organic carbon from the central equatorial Pacific determined using a combined drifting trap-^{234}Th approach. *Deep Sea Research, Part II*, *43*(4-6), 1095–1132. https://doi.org/10.1016/0967-0645(96)00036-7

Nowald, N., Iversen, M. H., Fischer, G., Ratmeyer, V., & Wefer, G. (2015). Time series of in-situ particle properties and sediment trap fluxes in the coastal upwelling filament off Cape Blanc, Mauritania. *Progress in Oceanography*, *137*, 1–137, 11. https://doi.org/10.1016/j.pocean.2014.12.015

Nozaki, Y., Thomson, J., & Turekian, K. K. (1976). The distribution of ^{210}Pb and ^{210}Po in the surface waters of the Pacific Ocean. *Earth and Planetary Science Letters*, *32*(2), 304–312. https://doi.org/10.1016/0012-821X(76)90070-4

Ohnemus, D. C. (2014). The biogeochemistry of marine particulate trace metals, (PhD Dissertation, p. 180). MIT-WHOI. Retrieved from http://hdl.handle.net/1721.1/87512, https://doi.org/10.1575/1912/6353

Ohnemus, D. C., & Lam, P. J. (2015). Cycling of lithogenic marine particles in the US GEOTRACES North Atlantic transect. *Deep Sea Research, Part II*, *116*, 283–302. https://doi.org/10.1016/j.dsr2.2014.11.019

Ohnemus, D. C., Rauschenberg, S., Cutter, G. A., Fitzsimmons, J. N., Sherrell, R. M., & Twining, B. S. (2017). Elevated trace metal content of prokaryotic communities associated with marine oxygen deficient zones. *Limnology and Oceanography*, *62*(1), 3–25. https://doi.org/10.1002/lno.10363

Okubo, A., Obata, H., Luo, S., Gamo, T., Yamamoto, Y., Minami, H., & Yamada, M. (2007). Particle flux in the twilight zone of the eastern Indian Ocean: A constraint from ^{234}U-^{230}Th and ^{228}Ra-^{228}Th disequilibria. *Deep Sea Research, Part I*, *54*(10), 1758–1772. https://doi.org/10.1016/j.dsr.2007.06.009

Owens, S. A., Buesseler, K. O., & Sims, K. W. W. (2011). Re-evaluating the ^{238}U-salinity relationship in seawater: Implications for the U–^{234}Th disequilibrium method. *Marine Chemistry*, *127*(1-4), 31–39. https://doi.org/10.1016/j.marchem.2011.07.005

Owens, S. A., Pike, S., & Buesseler, K. O. (2015). Thorium-234 as a tracer of particle dynamics and upper ocean export in the Atlantic Ocean. *Deep Sea Research, Part II*, *116*, 42–59. https://doi.org/10.1016/j.dsr2.2014.11.010

Pates, J. M., & Muir, G. K. P. (2007). U–salinity relationships in the Mediterranean: Implications for Th:^{238}U particle flux studies. *Marine Chemistry*, *106*(3-4), 530–545. https://doi.org/10.1016/j.marchem.2007.05.006

Pavia, F., Anderson, R., Vivancos, S., Fleisher, M., Lam, P., Lu, Y., et al. (2018). Intense hydrothermal scavenging of ^{230}Th and ^{231}Pa in the deep Southeast Pacific. *Marine Chemistry*, *201*, 212–228. https://doi.org/10.1016/j.marchem.2017.08.003

Peterson, M. L., Hernes, P. J., Thoreson, D. S., Hedges, J. I., & Lee, C. (1993). Field evaluation of a varved sediment trap. *Limnology and Oceanography*, *38*(8), 1741–1761. https://doi.org/10.4319/lo.1993.38.8.1741

Primeau, F. (2005). Characterizing transport between the surface mixed layer and the ocean interior with a forward and adjoint global ocean transport model. *Journal of Physical Oceanography*, *35*(4), 545–564. https://doi.org/10.1175/JPO2699.1

Puigcorbé, V., Roca-Martí, M., Masqué, P., Benitez-Nelson, C., Rutgers van der Loeff, M., Bracher, A., & Moreau, S. (2017). Latitudinal distributions of particulate carbon export across the North Western Atlantic Ocean. *Deep Sea Research, Part I*, *129*, 116–130. https://doi.org/10.1016/j.dsr.2017.08.016

Rigaud, S., Stewart, G., Baskaran, M., Marsan, D., & Church, T. (2015). ^{210}Po and ^{210}Pb distribution, dissolved-particulate exchange rates, and particulate export along the North Atlantic US GEOTRACES GA03 section. *Deep Sea Research, Part II*, *116*, 60–78. https://doi.org/10.1016/j.dsr2.2014.11.003

Roy-Barman, M. (2009). Modelling the effect of boundary scavenging on thorium and protactinium profiles in the ocean. *Biogeosciences*, *6*(12), 3091–3107. https://doi.org/10.5194/bg-6-3091-2009

Rutgers van der Loeff, M., Cai, P., Stimac, I., Bauch, D., Hanfland, C., Roeske, T., & Moran, S. B. (2012). Shelf-basin exchange times of Arctic surface waters estimated from ^{228}Th/^{228}Ra disequilibrium. *Journal of Geophysical Research*, *117*, C03024. https://doi.org/10.1029/2011JC007478

Saito, M. A., Noble, A. E., Hawco, N., Twining, B. S., Ohnemus, D. C., John, S. G., et al. (2017). The acceleration of dissolved cobalt's ecological stoichiometry due to biological uptake, remineralization, and scavenging in the Atlantic Ocean. *Biogeosciences*, *14*(20), 4637–4662. https://doi.org/10.5194/bg-14-4637-2017

Savoye, N., Benitez-Nelson, C., Burd, A. B., Cochran, J. K., Charette, M., Buesseler, K. O., et al. (2006). Th sorption and export models in the water column: A review. *Marine Chemistry*, *100*(3-4), 234–249. https://doi.org/10.1016/j.marchem.2005.10.014

Scholten, J. C., Fietzke, J., Vogler, S., Rutgers van der Loeff, M. M., Mangini, A., Koeve, W., et al. (2001). Trapping efficiencies of sediment traps from the deep eastern North Atlantic: The ^{230}Th calibration. *Deep Sea Research, Part II*, *48*(10), 2383–2408. https://doi.org/10.1016/S0967-0645(00)00176-4

Shannon, L. V., Cherry, R. D., & Orren, M. J. (1970). Polonium-210 and lead-210 in the marine environment. *Geochimica et Cosmochimica Acta*, *34*(6), 701–711. https://doi.org/10.1016/0016-7037(70)90072-4

Sherrell, M., & Boyle, A. (1992). The trace metal composition of suspended particles in the oceanic water column near Bermuda. *Earth and Planetary Science Letters*, *111*, 155–174.

Smith, J. N., Yeats, P. A., Knowlton, S. E., & Moran, S. B. (2014). Comparison of ^{234}Th/^{238}U and mass balance models for estimating metal removal fluxes in the Gulf of Maine and Scotian shelf. *Continental Shelf Research*, *77*, 107–117. https://doi.org/10.1016/j.csr.2014.01.008

Stewart, G., Cochran, J. K., Miquel, J. C., Masqué, P., Szlosek, J., Rodriguez y Baena, A. M., et al. (2007). Comparing POC export from ^{234}Th/^{238}U and ^{210}Po/^{210}Pb disequilibria with estimates from sediment traps in the northwest Mediterranean. *Deep Sea Research, Part I*, *54*(9), 1549–1570. https://doi.org/10.1016/j.dsr.2007.06.005

Stewart, G. M., Fowler, S. W., Teyssie, J. L., Cotret, O., Cochran, J. K., & Fisher, N. S. (2005). Contrasting transfer of polonium-210 and lead-210 across three trophic levels in marine plankton. *Marine Ecology Progress Series*, *290*, 27–33. https://doi.org/10.3354/meps290027

Sweeney, E. N., Mcgillicuddy, D. J., & Buesseler, K. O. (2003). Biogeochemical impacts due to mesoscale eddy activity in the Sargasso Sea as measured at the Bermuda Atlantic Time-series Study (BATS). *Deep Sea Research, Part II*, *50*(22-26), 3017–3039. https://doi.org/10.1016/j.dsr2.2003.07.008

Tang, Y., Stewart, G., Lam, P. J., Rigaud, S., & Church, T. (2017). The influence of particle concentration and composition on the fractionation of ^{210}Po and ^{210}Pb along the North Atlantic GEOTRACES transect GA03. *Deep Sea Research, Part I*, *128*, 42–54. https://doi.org/10.1016/j.dsr.2017.09.001

Turekian, K. K., Nozaki, Y., & Benning, L. K. (1977). Geochemistry of atmospheric radon and radon products. *Annual Review of Earth and Planetary Sciences*, *5*(1), 227–255. https://doi.org/10.1146/annurev.ea.05.050177.001303

Twining, B. S., Rauschenberg, S., Morton, P. L., Ohnemus, D. C., & Lam, P. J. (2015). Comparison of particulate trace element concentrations in the North Atlantic Ocean as determined with discrete bottle sampling and in situ pumping. *Deep Sea Research, Part II*, *116*, 273–282. https://doi.org/10.1016/j.dsr2.2014.11.005

Twining, B. S., Rauschenberg, S., Morton, P. L., & Vogt, S. 2015. Metal contents of phytoplankton and labile particulate material in the North Atlantic Ocean. Prog. Oceanogr. *137*, 261–283. https://doi.org/10.1016/j.pocean.2015.07.001

Verdeny, E., Masque, P., Garcia-Orellana, J., Hanfland, C., Cochran, J. K., & Stewart, G. M. (2009). POC export from ocean surface waters by means of ^{234}Th/^{238}U and ^{210}Po/^{210}Pb disequilibria: A review of the use of two radiotracer pairs. *Deep Sea Research, Part II*, *56*(18), 1502–1518. https://doi.org/10.1016/j.dsr2.2008.12.018

Weber, T., Cram, J. A., Leung, S. W., DeVries, T., & Deutsch, C. (2016). Deep ocean nutrients imply large latitudinal variation in particle transfer efficiency. *Proceedings of the National Academy of Sciences*, *113*(31), 8606–8611. https://doi.org/10.1073/pnas.1604414113

Weinstein, S. E., & Moran, S. B. (2005). Vertical flux of particulate Al, Fe, Pb, and Ba from the upper ocean estimated from ^{234}Th/^{238}U disequilibria. *Deep Sea Research, Part I*, *52*(8), 1477–1488. https://doi.org/10.1016/j.dsr.2005.03.008

Yu, E., Francois, R., Bacon, M. P., Honjo, S., Fleer, A. P., Manganini, S. J., et al. (2001). Trapping efficiency of bottom-tethered sediment traps estimated from the intercepted fluxes of ^{230}Th and ^{231}Pa. *Deep Sea Research, Part I*, *48*(3), 865–889. https://doi.org/10.1016/S0967-0637(00)00067-4